FROM CANONICAL TO ENHANCED EXTRA MIXING IN LOW-MASS RED GIANTS: TIDALLY LOCKED BINARIES

Pavel A. Denissenkov[1,2,3], Brian Chaboyer[1], & Ke Li[1]

ABSTRACT

Stellar models which incorporate simple diffusion or shear induced mixing are used to describe canonical extra mixing in low mass red giants of low and solar metallicity. These models are able to simultaneously explain the observed Li and CN abundance changes along upper red giant branch (RGB) in field low-metallicity stars and match photometry, rotation and $^{12}C/^{13}C$ ratios for stars in the old open cluster M67. The shear mixing model requires that main sequence (MS) progenitors of upper RGB stars possessed rapidly rotating radiative cores and that specific angular momentum was conserved in each of their mass shells during their evolution. We surmise that solar-type stars will not experience canonical extra mixing on the RGB because their more efficient MS spin-down resulted in solid-body rotation, as revealed by helioseismological data for the Sun. Thus, RGB stars in the old, high metallicity cluster NGC 6791 should show no evidence for mixing in their $^{12}C/^{13}C$ ratios.

We develop the idea that canonical extra mixing in a giant component of a binary system may be switched to its enhanced mode with much faster and somewhat deeper mixing as a result of the giant's tidal spin-up. This scenario can explain photometric and composition peculiarities of RS CVn binaries. The tidally enforced enhanced extra mixing might contribute to the star-to-star abundance variations of O, Na and Al in globular clusters. This idea may be tested with observations of $^{12}C/^{13}C$ ratios and CN abundances in RS CVn binaries.

Subject headings: stars: chemically peculiar — stars: evolution — stars: interiors — stars: late-type — stars: rotation — globular clusters: general

[1]Department of Physics & Astronomy, Dartmouth College, 6127 Wilder Laboratory, Hanover, NH 03755-3528, USA; Brian.Chaboyer@Dartmouth.edu, Ke.Li@Dartmouth.edu.

[2]Present address: Department of Astronomy, The Ohio State University, 4055 McPherson Laboratory, 140 West 18th Avenue, Columbus, OH 43210; dpa@astronomy.ohio-state.edu.

[3]On leave from Sobolev Astronomical Institute of St. Petersburg State University, Universitetsky Pr. 28, Petrodvorets, 198504 St. Petersburg, Russia.

1. Introduction

Standard stellar evolution models assume that mixing only occurs in convective regions of stars. However, there is convincing evidence that a majority of low-mass ($0.8 \lesssim M/M_\odot \lesssim 2$) stars are experiencing nonconvective *extra mixing* on the upper red giant branch (RGB) (e.g., Sweigart & Mengel 1979; Langer et al. 1986; Sneden et al. 1986; VandenBerg & Smith 1988; Smith & Tout 1992; Charbonnel 1994, 1995; Charbonnel, Brown & Wallerstein 1998; Charbonnel & do Nascimento 1998; Gratton et al. 2000; Bellman et al. 2001; Grundahl et al. 2002; Denissenkov & VandenBerg 2003a; Smith & Martell 2003; Shetrone 2003). These red giants have a helium electron-degenerate core, a hydrogen burning shell (HBS) atop the core, and a thin radiative zone between the HBS and the bottom of the convective envelope (BCE) (Fig. 1). The most convincing observational evidence of mixing in red giants is the evolution of their surface carbon isotopic ratio ^{12}C/^{13}C and abundances $\log \varepsilon(^7$Li), [C/Fe] and [N/Fe][1] with increasing luminosity L along the RGB (*circles* in Fig. 2). The first abundance changes that occur on the subgiant and lower red giant branch ($0.6 \lesssim \log L/L_\odot \lesssim 1.0$) are produced by the deepening BCE during the standard first dredge-up episode (Iben 1967). Here, the convective envelope engulfs the stellar layers in which the CN-cycle had altered the relative abundances of ^{12}C, ^{13}C and N while on the main sequence (MS). Convection also dilutes the envelope abundance of Li that has survived only in a thin subsurface layer where the temperature was less than $\sim 2.5 \times 10^6$ K. At the end of the first dredge-up, the BCE stops to deepen and begins to retreat. It leaves a discontinuity of the chemical composition at the level of its deepest penetration. The evolutionary changes of the surface element abundances resume precisely at the moment when the HBS, advancing in mass inside red giants, erases the composition discontinuity left behind by the BCE. The commonly accepted interpretation of this is based on the following assumptions: (1) some extra mixing is present in the red giants' radiative zones; (2) it connects the BCE with the layers adjacent to the HBS (Fig. 1), where the CN-cycle is at work and Li is strongly depleted, thus dredging up stellar material enriched in N and deficient in C and Li; (3) at lower luminosities, extra mixing is shielded from reaching the vicinity of the HBS by a large gradient of the mean molecular weight (a μ-gradient barrier) built up by the composition discontinuity (Charbonnel, Brown & Wallerstein 1998; Denissenkov & VandenBerg 2003a).

When the HBS meets and erases the μ-gradient barrier, the evolution of red giants slows down for a while. This results in prominent bumps in the differential luminosity functions of globular clusters, which have really been observed (e.g., Zoccali et al. 1999; Monaco et al.

---

[1] We use the standard spectroscopic notations: $[A/B] = \log(N(A)/N(B)) - \log(N(A)/N(B))_\odot$, where $N(A)$ and $N(B)$ are number densities of the nuclides A and B; $\log \varepsilon(^7$Li$) = \log(N(^7$Li$)/N(H)) + 12$.

2002; Cassisi et al. 2002; Salaris et al. 2002; Riello et al. 2003). Therefore, the luminosity at which extra mixing starts to manifest itself (at $\log L/L_\odot \approx 1.8 - 2.0$ in Fig. 2) is called "the bump luminosity". It divides the RGB into its lower and upper part. In stars with $M \gtrsim 2\,M_\odot$, the HBS fails to cross the μ-gradient barrier before the core helium ignition is triggered. In concordance with this, no manifestations of extra mixing have been reported in intermediate-mass red giants (Gilroy 1989).

In the absence of a reliable theory of extra mixing in upper RGB stars, semi-empirical models are worth applying. In particular, a simple diffusion model has shown that in the majority of upper RGB stars the depth and rate of extra mixing do not seem to vary greatly from star to star. According to Denissenkov & VandenBerg (2003a), these quantities can be parameterized by any pair of correlated values within the close limits specified by $\Delta \log T \approx 0.19$ and $D_{\mathrm{mix}} \approx 4 \times 10^8\,\mathrm{cm^2\,s^{-1}}$, to $\Delta \log T \approx 0.22$ and $D_{\mathrm{mix}} \approx 8 \times 10^8\,\mathrm{cm^2\,s^{-1}}$. Here, $\Delta \log T$ is a difference between the logarithms of temperature at the base of the HBS and at a specified maximum depth of extra mixing M_{mix} (Fig. 1), and D_{mix} is a constant diffusion coefficient.

Given that the majority of metal-poor upper RGB stars, both in the field and in globular clusters, experience extra mixing with almost the same depth and rate, Denissenkov & VandenBerg (2003a) have proposed to call this universal process "canonical extra mixing". Although its physical mechanism is not identified yet, the phenomenon of Li-rich K-giants and its interpretation are likely to support a rotational mechanism. Indeed, most of the Li-rich giants are located above the bump luminosity (Charbonnel & Balachandran 2000). Their proportion among rapid rotators ($v \sin i \geq 8\ \mathrm{km\,s^{-1}}$) is $\sim 50\%$. Compare this to $\sim 2\%$ of Li-rich stars among the much more common slowly rotating ($v \sin i \lesssim 1\ \mathrm{km\,s^{-1}}$) K-giants (Drake et al. 2002). Because for extra mixing driven by kinetic energy of rotation $D_{\mathrm{mix}} \propto v^2$, a tenfold increase of v would enhance D_{mix} from its canonical value of $\sim 10^9\ \mathrm{cm^2\,s^{-1}}$ to $\sim 10^{11}\ \mathrm{cm^2\,s^{-1}}$. Denissenkov & Herwig (2004) have shown that precisely such enhancement of D_{mix} is required to produce Li in K-giants via the ^{7}Be-mechanism (Cameron & Fowler 1971). Therefore, following Denissenkov & VandenBerg (2003a), we hypothesize that sometimes, when an upper RGB star gets spun up by an external source of angular momentum, the presumably rotational extra mixing in its radiative zone may switch from its canonical mode to *an enhanced mode* with much faster and somewhat deeper mixing.

Denissenkov & Weiss (2000) have proposed that single Li-rich giants might have been spun up by engulfed massive planets. Alternatively, a red giant can be spun up by a close stellar companion. In this case, its rotation is accelerated by a drag force originating from viscous dissipation of kinetic energy of a tidal hump raised in its convective envelope by a companion star. As a result of this interaction, spin and orbital rotation of the red giant

get synchronized, and its initially elliptical orbit can become circular. Fig. 3 illustrates tidal synchronization in real stars. Here, we have plotted observational data of De Medeiros et al. (2002) on projected rotational velocities $v \sin i$ and orbital periods P of G and K giant components of field binaries with available orbital parameters. The values of $v \sin i$ were multiplied by the factor $4/\pi \approx 1.27$ that takes into account a random orientation of the stars' axes of rotation. *Filled circles* are binary systems with a circular or nearly circular orbit (those with eccentricities $e \leq 0.10$). Systems with eccentric orbits ($e > 0.10$) are represented by *open circles*. A set of theoretical curves is constructed by us under the assumption that $\Omega = \omega$, where Ω and ω are the spin and orbital angular velocity of a red giant, for 4 values of the red giant's radius: $R/R_\odot = 5$, 10, 20 and 40 (*solid curves* from left to right). The tidal circularization time is longer than the synchronization time (e.g., Hurley et al. 2002), therefore the giants represented by filled circles are most likely to have synchronized their rotation.

The goal of this paper is twofold. First, in §3 we demonstrate that canonical extra mixing in solar-metallicity red giants in the open cluster M67 can be modeled using essentially the same parameters as those adjusted for metal-poor stars. After that, we attempt to model enhanced extra mixing in red giant components of tidally locked (corotating) binaries that are spun up as a result of tidal synchronization between their spin and orbital rotation (§4). In order to get a self-consistent picture of switching from canonical to enhanced extra mixing, in §4 we make assumptions and use Ω–profiles and parameters of extra mixing compatible with those discussed in §3. Finally, §5 contains a summary of our main conclusions along with a proposal of observational tests that could confirm or reject our models.

2. Stellar Evolution Code with Rotation and Extra Mixing

Evolution of rotating stellar models with extra mixing on the upper RGB is calculated from the zero-age MS (ZAMS) to the RGB tip with an upgraded version of the computer code used by Denissenkov & VandenBerg (2003a,b). The most recent update is the adoption of Alan Irwin's improved EOS[2]. In addition, the energy losses due to neutrino emission are now calculated with the code distributed by Itoh et al. (1996). Our stellar evolution code uses OPAL opacities (Rogers & Iglesias 1992) for temperatures above $\sim 10^4$ K, complemented by Alexander & Ferguson (1994) data for lower temperatures: both datasets assume solar abundances of α–elements. With the new EOS, we use a value of $l_{\mathrm{conv}}/H_P = 1.75$ for the

---

[2]We use the EOS code that is made publicly available at `ftp://astroftp.phys.uvic.ca/pub/irwin/eos/code/eos_demo_fortran.tar.gz` under the GNU General Public License.

ratio of the convective mixing length to the pressure scale height derived from a calibrated solar model.

In our MS models with $M > 1\,M_\odot$, some overshooting has been introduced beyond the formal convective core border determined by the Schwarzschild criterion by assuming that the ratio of the radiative and adiabatic temperature gradients (logarithmic and with respect to pressure) at the core border $\nabla_{\rm rad}/\nabla_{\rm ad} = 0.9$ instead of 1. Using this approach, we succeeded in fitting our solar-metallicity 4×10^9 yr isochrone[3] (Fig. 4, *solid curve*) for the high precision color-magnitude diagram (CMD) of M67 published by Sandquist (2004) (Fig. 4, *open circles*). We ignored any microscopic mixing, such as atomic diffusion, gravitational settling and radiative levitation.

The treatment of extra mixing in the radiative zones separating the BCE from the HBS is the same as that described by Denissenkov & VandenBerg (2003a, see their equation (1)). Effects of shellular rotation on the internal structure and evolution of stars are treated in the same way as by Denissenkov & VandenBerg (2003b). The code employed in this work only considers the simplest cases of the angular momentum profile evolution: either (a) supporting the uniform (solid-body) rotation, $\Omega(t, M_r) = \Omega(t)$, or (b) keeping the constant specific angular momentum in each mass shell, including convective regions, $j(t, M_r) \equiv \frac{2}{3}r^2\Omega = j(0, M_r)$. These two opposite cases correspond to a maximum possible and a zero efficiency of the angular momentum redistribution throughout a star.

3. Canonical Extra Mixing in Single Red Giants of Solar Metallicity

In this section, we present results of our new stellar evolution computations that, when being compared with recent observational data on photometry, rotation and chemical composition of Population I (in the open cluster M67) and Population II (both in the field and in globular clusters) low-mass stars, allow to constrain the strength of rotation-induced shear mixing.

3.1. Basic Equations and Assumptions in the Shear Mixing Model

When studying the evolution of metal-poor stars with $M \approx 0.9\,M_\odot$, Denissenkov & Tout (2000) and Denissenkov & VandenBerg (2003a) have proposed that canonical extra

---

[3]Necessary bolometric corrections and $T_{\rm eff}$ – color transformations were calculated with a code kindly presented to one of us (PAD) by Don VandenBerg.

mixing in upper RGB stars can be identified with turbulent diffusion induced by secular shear instability in their differentially rotating radiative zones and that it can be modeled using the coefficient of vertical turbulent diffusion derived by Maeder & Meynet (1996)

$$D_{\mathrm{v}} = f_{\mathrm{v}} \times 8 Ri_{\mathrm{c}} \frac{K}{N_T^2} \left[\frac{1}{5} \Omega^2 \left(\frac{\partial \ln \Omega}{\partial \ln r} \right)^2 - N_\mu^2 \right]. \tag{1}$$

Here,

$$N_T^2 = \frac{g\delta}{H_P} (\nabla_{\mathrm{ad}} - \nabla_{\mathrm{rad}}), \quad \text{and} \quad N_\mu^2 = g\varphi \left| \frac{\partial \ln \mu}{\partial r} \right|$$

are the T- and μ-components of the square of the Brunt–Väisälä (buoyancy) frequency, g is the local gravity, $Ri_{\mathrm{c}} = \frac{1}{4}$ is the classical critical Richardson number, and

$$K = \frac{4acT^3}{3\kappa\rho^2 C_P} \tag{2}$$

is the thermal diffusivity with κ and C_P representing the opacity and the specific heat at constant pressure, respectively. The quantities $\delta = -\left(\partial \ln \rho / \partial \ln T \right)_{P,\mu}$ and $\varphi = \left(\partial \ln \rho / \partial \ln \mu \right)_{P,T}$ are determined by the equation of state.

Equation (1) gives simultaneously the extra mixing rate

$$D_{\mathrm{mix}} \approx f_{\mathrm{v}} \times \frac{8}{5} Ri_{\mathrm{c}} \frac{K}{N_T^2} \Omega^2 \left(\frac{\partial \ln \Omega}{\partial \ln r} \right)^2 \tag{3}$$

and depth M_{mix}, the latter being determined as the coordinate of the first mass shell beneath the BCE where $D_{\mathrm{v}} = 0$, or

$$N_\mu^2 \equiv g\varphi \left| \frac{\partial \ln \mu}{\partial r} \right| = \frac{1}{5} \Omega^2 \left(\frac{\partial \ln \Omega}{\partial \ln r} \right)^2. \tag{4}$$

Although the depth given by equation (4) for reasonable Ω–profiles is surprisingly close to that specified by the parameter $\Delta \log T = 0.19 - 0.22$ in our simple diffusion model, the rate calculated with equation (3) when $f_{\mathrm{v}} = 1$ is found to be too slow for canonical extra mixing (Denissenkov & VandenBerg 2003a). Therefore, we have to insert *an enhancement factor* $f_{\mathrm{v}} \gg 1$ into equations (1) and (3).

For the low values of $v \sin i$ usually measured in MS stars with $M \lesssim 1 M_\odot$, rotational mixing, such as meridional circulation or turbulent diffusion, can reproduce the evolutionary changes of [C/Fe] in their upper RGB descendants only assuming that the specific angular momentum is conserved in each mass shell of these stars during their entire evolution from the ZAMS to the RGB tip (Sweigart & Mengel 1979; Smith & Tout 1992; Denissenkov &

Tout 2000; Denissenkov & VandenBerg 2003a). Even having assumed that, some differential rotation in the initial models is still required. Following Denissenkov & VandenBerg (2003a,b), we set up such differential rotation in our ZAMS models assuming that the ratio of the equatorial centrifugal acceleration to the gravity is constant along the radius and that it is a small fraction of the critical ratio for the Roche potential used in our rotating stellar models; i.e.,

$$\varepsilon(M_r) \equiv \frac{r^3 \Omega^2}{3GM_r} = f_\varepsilon \, \varepsilon_{\mathrm{crit}} = \mathrm{constant}, \tag{5}$$

where $\varepsilon_{\mathrm{crit}} \approx 0.24$. The ratio of the angular velocity near the center to Ω at the surface obtained in this way is less than 10 for all of the ZAMS models considered below. Thus, we admit that the solid-body rotation of the inner Sun as revealed by helioseismological data (e.g., Chaplin et al. 1999) may not necessarily be applicable to all low-mass MS stars. The free parameter f_ε is chosen so as to get theoretical values of v_{rot} close to projected rotational velocities of MS and subgiant stars. After that we evolve our models from the ZAMS to the bump luminosities keeping j constant in every mass shell. No extra mixing is allowed in the models until they will reach the bump luminosities. For the sake of simplicity, we ignore mass loss (in fact, it becomes important only in the very vicinity of the RGB tip).

3.2. A Summary of Results for the Single Star Case

Equations (4) and (3) with values of Ω and $(\partial \ln \Omega / \partial \ln r)$ taken from the radiative zones of our bump luminosity models give approximately the same depths of extra mixing and diffusion coefficients that are only $\sim 15 - 25$ times as small as those constrained by our semi-empirical diffusion model. This conclusion is true not only for metal-poor low-mass stars, as was anticipated by Denissenkov & VandenBerg (2003a), but also for their solar-metallicity counterparts. To demonstrate this, we have computed the evolution of three rotating stellar models: the first two for the same mass $M = 0.85 \, M_\odot$ and helium abundance $Y = 0.24$ but for two different heavy-element mass fractions $Z = 0.002$ and $Z = 0.0005$, and the third model for $M = 1.35 \, M_\odot$, hydrogen abundance $X = 0.70$ and the solar value of $Z = 0.0188$.

The initial rotation profiles of the first two models have been specified by the parameter $f_\varepsilon = 0.0003$. This results in surface equatorial rotational velocities v_{rot} monotonously decreasing from $\sim 7 \, \mathrm{km \, s^{-1}}$ to $\sim 4 \, \mathrm{km \, s^{-1}}$ during the models' MS lives. When these metal-poor models leave the MS and become subgiants, their rotation slows down to $v_{\mathrm{rot}} \leq 4 \, \mathrm{km \, s^{-1}}$ due to a surface radius increase (Fig. 5, *solid curve*). Similar values of "true" mean rotational velocities have been measured in the MS turnoff and subgiant stars in the globular clusters

NGC 104, NGC 6397 and NGC 6752 by Lucatello & Gratton (2003) (*squares with errorbars in Fig. 5*). The third model evolves along the RGB of the 4×10^9 yr isochrone that matches the CMD of the old solar-metallicity open cluster M67 (Fig. 4, *dashed curve*). For this model, the parameter $f_\varepsilon = 0.00075$ has been chosen so as the computed behavior of $v_{\rm rot}$ along the rotational isochrone of the same age constructed using stellar models with $M \geq 1.1\,M_\odot$ and the same parameter f_ε (Fig. 6, *solid curve*) to be in a qualitative agreement with the observed decrease of $(4/\pi)v\sin i$ in the M67 stars whose evolutionary status changes from the MS to the subgiant branch (Fig. 6, *circles*). Unfortunately, at present we cannot discriminate between the cases of differential and solid-body rotation of M67 stars (compare *solid* and *short-dashed curves* in Fig. 6). However, the observational data in Fig. 6 seem to support our assumption of slow surface rotation ($v_{\rm rot} \approx 10$ km s^{-1}) of M67 stars on the early MS (compare *solid* and *short-dashed curves* with *dot-long-dashed* and *long-dashed curves*). The stars from Fig. 6 are also plotted in Fig. 4 as *filled circles*. Comparison of these two figures shows that the stars with $(B-V)_0 \approx 0.55-0.60$ in Fig. 6 have $M < 1.35\,M_\odot$. Their masses are probably close to the M67 MS turn-off mass, which is $M \approx 1.25\,M_\odot$. Only the objects with $(B-V)_0 \gtrsim 0.9$ in Fig. 6 are subgiants and lower RGB stars having $M \approx 1.35\,M_\odot$.

In Fig. 7, *vertical dotted and dashed line segments* in panels d indicate depths specified by $\Delta \log T = 0.19$ and 0.22 in the third ($M = 1.35\,M_\odot$, $Z = 0.0188$) unmixed model that is located immediately above its bump luminosity. *Solid line segment* points to the mixing depth calculated with equation (4) using an Ω–profile extracted from the same stellar model. Note the proximity of the broken and solid line segments.

Starting from the bump luminosity models, we continue our stellar evolution computations. Rotational shear mixing described by equation (1) is now taken into account. To be more exact, we introduce a diffusion coefficient $D_{\rm mix} = D_{\rm v}$ for $D_{\rm v} > 0$ while letting $D_{\rm mix} = 0$ for $D_{\rm v} \leq 0$. A new Ω–profile required to recalculate $D_{\rm v}$ is taken from the evolving rotating stellar models in each time step. As in the models below the bump luminosities, the specific angular momentum is still assumed to remain constant in each mass shell, including convective envelopes. Thus, our new extra mixing computations include for the first time both a plausible physical description for the diffusion coefficient $D_{\rm mix}$, with its profile allowed to change along the whole length of upper RGB[4], and a feedback effect of rotation and chemical mixing on the structure and evolution of red giants. In order to simulate the evolutionary variations of the surface ^{12}C/^{13}C ratio and abundances of Li, C and N in the field metal-poor upper RGB stars we had to increase by a factor of $f_{\rm v} = 15-25$ the value of $D_{\rm v}$ given by Maeder & Meynet (1996) in our $0.85\,M_\odot$ rotating models (Fig. 2). At the same time, the

---

[4]Denissenkov & VandenBerg (2003a) used a fixed $D_{\rm mix}$-profile proportional to $D_{\rm v}$ in the bump luminosity model.

^{12}C/^{13}C ratios in a couple of upper RGB stars and in a few clump stars in the cluster M67 were reproduced by our $1.35\,M_\odot$ model only after $D_{\rm v}$ had been multiplied by $f_{\rm v} = 15$ (Fig. 8, *dashed curve*). For comparison, *dotted curve* in Fig. 8 has been computed with the diffusion model using $\Delta \log T = 0.22$ and $D_{\rm mix} = 8 \times 10^8\,{\rm cm^2\,s^{-1}}$. Also, compare our Fig. 2 with Fig. 4 from Denissenkov & VandenBerg (2003a). The ratio between the enhancement factors 25 and 15, adjusted for the low-mass red giant models of different metallicities, is even smaller than the one between our empirically constrained limits for the diffusion coefficient: $D_{\rm mix} = 8 \times 10^8\,{\rm cm^2\,s^{-1}}$ and $D_{\rm mix} = 4 \times 10^8\,{\rm cm^2\,s^{-1}}$.

Fig. 7 shows element abundance profiles, μ-gradients and diffusivities for two rotating stellar models with $M = 1.35\,M_\odot$, $Z = 0.0188$ and $f_\varepsilon = 0.00075$ located close to their bump luminosity. Compared to the case of metal-poor red giants, the only important qualitative distinction here is the additional hump in the μ-gradient profile at $M_r/M_\odot \approx 0.2535$ in the upper RGB model clearly seen in panel d. It is built up by H abundance variations that accompany the ^{12}C to ^{14}N transformation (see panel b). Because of this hump, the vertical turbulent diffusion cannot approach as close to the HBS as in the low-metallicity case. It can hardly reach a peak in the ^{13}C abundance profile (panel b). At the same location, the ^{12}C depletion just sets in. This may explain why in the solar-metallicity case canonical extra mixing only produces modest changes of the surface ^{12}C/^{13}C ratio (Fig. 8).

To summarize, multiplying the diffusion coefficient $D_{\rm v}$ from Maeder & Meynet (1996) by a factor of $f_{\rm v} = 20 \pm 5$, we can satisfactorily reproduce the observed evolutionary variations of the surface ^{12}C/^{13}C isotopic ratio and abundances of Li, C and N in the field metal-poor upper RGB stars (Fig. 2) as well as the scanty ^{12}C/^{13}C data for the upper RGB and clump stars in the old solar-metallicity open cluster M67 (Fig. 8). This can only be done under the assumption of differential rotation both in the low-mass MS ancestors of these evolved stars and in the convective envelopes of red giants. Otherwise, one has to search for an alternative mechanism of canonical extra mixing.

Interestingly, our two models of canonical extra mixing (the diffusion model and the shear instability model) predict qualitatively different evolutionary changes of the surface Li abundance near the RGB tip. Whereas in the first model $\log \varepsilon(^7{\rm Li})$ remains very low, in the second model $\log \varepsilon(^7{\rm Li})$ resumes its post-first-dredge-up value and even exceeds it towards the RGB tip (compare upper panels in our Fig. 2 and in Fig. 4 from Denissenkov & VandenBerg (2003a)). This difference is due to a considerable increase of the diffusion coefficient $D_{\rm v} \propto K$ (equation (1)) in the second model caused by a growth of the thermal diffusivity K with the luminosity and the assumed constancy of $D_{\rm mix}$ in the first model. The larger diffusion coefficient leads to some Li production via the ^{7}Be-mechanism. This new result can explain the higher Li abundances in clump stars compared to those in red giants

discussed by Pasquini et al. (2001).

Now, we want to comment on the required enhancement of $D_{\rm v}$. We can formally comply with this requirement by choosing a value of the critical Richardson number $Ri_{\rm c}$ larger than $\frac{1}{4}$ instead of taking $f_{\rm v} \gg 1$. Indeed, the modern models of shear-driven turbulence do predict that $Ri_{\rm c}$ should be at least 4 (Canuto 2002) or even 6.4 (Brüggen & Hillebrandt 2001) times as large as its classical value. If we accept this then the enhancement factor $f_{\rm v}$ in equation (1) has only to be as large as $\sim 20/6.4 \approx 3$ for our model to reproduce the observations. It should also be noted that equation (1) takes into consideration only the largest turbulent eddies. Allowing for eddies from the whole turbulent spectrum would increase the coefficient $D_{\rm v}$ in a similar way as the Full Spectrum of Turbulence model (Canuto & Mazzitelli 1991) generates much more vigorous convection than the Mixing Length Theory.

As regarding the depth of shear mixing (4), it is directly constrained by the kinetic energy of differential rotation available to do work against the buoyancy force. It is our assumption of Ω increasing with depth in the convective envelopes of low-mass red giants and in their MS ancestors that allows shear mixing to approach close enough to the HBS. In order to reconcile this assumption with the well established fact of the Sun's solid-body rotation, we refer to the recent work of Talon & Charbonnel (2004), according to which, in a solar-type star, angular momentum can be extracted from its radiative core by internal gravity waves generated in its convective envelope. The efficiency of this process should depend on the thickness of convective envelope. Therefore, we hypothesize that rotation-induced extra mixing may only work in those red giants whose MS ancestors had shallower convective envelopes than the Sun. Indeed, both our ZAMS models, the one with $M = 1.35\,M_\odot$ and $Z = 0.0188$ and that with $M = 0.85\,M_\odot$ and $Z = 0.0005$ possess much thinner convective envelopes than the solar ZAMS model ($\log M_{\rm ce}/M_\odot = -3.92, -2.32$ and -1.62, respectively). Thus, we conjecture that metal-rich stars with $M \lesssim 1.2\,M_\odot$ might not experience canonical extra mixing on the RGB at all because their MS ancestors had thick surface convective zones and, as a result, nearly solid-body internal rotation, like the Sun. To test this hypothesis, it is necessary to determine $^{12}{\rm C}/^{13}{\rm C}$ ratios in upper RGB stars of an open cluster older than M67. A good candidate for these purposes is the open cluster NGC 6791. It has [Fe/H] $= +0.4$ and an age of $(8.0 \pm 0.5) \times 10^9$ yr (Chaboyer et al. 1999).

4. Enhanced Extra Mixing in Giant Components of Tidally Locked Binaries

Given that enhanced extra mixing is deeper than canonical one, it may penetrate the layers in outskirts of the HBS in which not only ^{12}C but also ^{16}O is depleted in the CNO cycle and where ^{23}Na is produced in the reaction $^{22}{\rm Ne}({\rm p},\gamma)^{23}{\rm Na}$ (Denissenkov & VandenBerg

2003a). Therefore, enhanced extra mixing in the extinct upper RGB stars that were slightly more massive ($0.9 \lesssim M/M_\odot \lesssim 2$) than the MS turn-off stars in the present-day globular clusters ($M \approx 0.8 - 0.9 \, M_\odot$) might have been one of the yet unidentified primordial sources of the global O–Na anticorrelation in globular cluster stars (Denissenkov & Weiss 2004).

For the binary star case, we consider two basic stellar models: a solar-metallicity one with $M = 1.7 \, M_\odot$, and a metal-poor one with $M = 1.0 \, M_\odot$ and $Z = 0.0005$. The first model has the mass and metallicity typical for both Li-rich K-giants and a sample of chromospherically active late-type giants — primaries of the RS Canum Venaticorum (CVn) binaries whose relevance to the problem of enhanced extra mixing will be discussed later. The second model represents a low-mass star that had completed its life in the past in a moderately metal-poor globular cluster. Both models will be "placed" into close binary systems with less massive stellar companions. Our main goal is to find out to what noticeable photometric and composition anomalies the tidal spin-up of these models may lead on the RGB.

4.1. Description of Tidal Interaction in a Binary System

4.1.1. Basic Equations

If the initial separation between low-mass stellar components of a binary system is too small then the primary star can fill its Roche lobe before having reached the RGB tip. In this case, the radius of the red giant primary has an upper limit constrained by the Roche lobe radius $R \leq R_L = E(q)a$, where a is the binary semi-major axis, $q = m/M$ is its mass ratio (secondary over primary), and, according to Eggleton (1983),

$$E(q) \approx \frac{0.49}{0.6 + q^{2/3} \ln(1 + q^{-1/3})}.$$

Dashed curve in Fig. 3 delineates the maximum surface rotational velocity of a red giant that fills its Roche lobe in a binary system with $M = 1.7 \, M_\odot$, $q = 0.5$, and an orbital period P, the latter being related to a via Kepler's third law

$$\left(\frac{a}{R_\odot}\right) = 4.207 P_{\mathrm{d}}^{2/3} \left(\frac{M}{M_\odot}\right)^{1/3} (1+q)^{1/3}, \tag{6}$$

where P_{d} is the period in days. We see that all stars but one lie below this curve. The only outlier is the G5 III star HD 21018. It has $v \sin i = 22.7 \; \mathrm{km \, s^{-1}}$, and the lithium abundance $\log \varepsilon(^7\mathrm{Li}) = 2.93$ (Hartoog 1978). It is most likely to be an intermediate-mass ($M \gtrsim 2.5 \, M_\odot$) star crossing the Hertzsprung gap on its way from the MS to the RGB region. Its location on the CMD (*asterisk* in Fig. 9) confirms our hypothesis. Thus, it may still preserve its

initial high Li abundance, while the large value of $v \sin i$ may be a signature of its previous fast rotation characteristic of the MS B-type stars.

In our work, the tidal evolution of orbital and rotational parameters of binary star systems is modeled using differential equations derived by Hut (1981). Hut has elaborated upon the weak friction model of Alexander (1973), which assumes that the tidal humps in a gravitationally distorted rotating star have their equilibrium shape, as described by Zahn (1977), but with a constant time lag between the moment when the tidally deformed equipotential surface has been formed in the absence of dissipation and the current binary star configuration. For the sake of simplicity, we only consider the tidal evolution of primary stars possessing convective envelopes in binary systems with the zero eccentricity. In this case, only the spin rotation of the primary and the binary semi-major axis are affected by the tidal interaction, their changes being controled by the following equations:

$$\frac{d\Omega}{dt} = 3\frac{k}{t_{\mathrm{F}}}\frac{q^2}{r_{\mathrm{g}}^2}\left(\frac{R}{a}\right)^6 (\omega - \Omega), \tag{7}$$

$$\frac{da}{dt} = -6\frac{k}{t_{\mathrm{F}}}q(1+q)\left(\frac{R}{a}\right)^8 a\frac{\omega - \Omega}{\omega}, \tag{8}$$

where

$$t_{\mathrm{F}} \approx t_{\mathrm{conv}} \approx \left(\frac{MR^2}{L}\right)^{1/3} = 0.4304\left[\frac{(M/M_\odot)(R/R_\odot)^2}{(L/L_\odot)}\right]^{1/3} \mathrm{yr} \tag{9}$$

is a characteristic time of viscous friction, which approximately equals the convective time scale (Zahn 1977) (friction experienced by the tidal humps is produced by the convective turbulent viscosity in the envelope), L is the primary star's luminosity, r_{g} is its radius of gyration that determines the total angular momentum $I = r_{\mathrm{g}}^2 MR^2$, Ω and ω are its spin and orbital angular velocities.

Equations (7−8) contain the apsidal motion constant of the primary

$$k = \frac{3 - \eta[a(R)]}{2\{2 + \eta[a(R)]\}}. \tag{10}$$

The structural function $\eta(a)$ can be obtained by integrating the differential equation of Radau (e.g. Claret & Willems 2002):

$$a\frac{d\eta}{da} + 6\frac{\rho}{\bar{\rho}}(\eta + 1) + \eta(\eta - 1) = 6 \tag{11}$$

with the boundary condition $\eta(0) = 0$. Here, $\rho(a)$ is the primary's density profile, and $\bar{\rho}(a)$ is the average density inside the equipotential surface (isobar) whose rotationally distorted

shape[5] is described as

$$r = a[1 - \varepsilon(a)P_2(\cos\theta)] \approx a,$$

where P_2 is the Legendre polynomial of order 2, θ is the colatitude, and

$$\varepsilon = \frac{\Omega(a)^2 a^3}{3GM_P}$$

is the ratio of the equatorial centrifugal acceleration to gravity divided by 3, with M_P being the mass inside the isobar P. The quantities η and ε are related to each other via $\eta = (d\ln\varepsilon/d\ln a)$.

The quantity ε has already been used to set up differential rotation in our ZAMS models (equation (5)). In our solar metallicity ZAMS model with $M = 1.7\,M_\odot$, the initial Ω–profile is specified by the same parameter $f_\varepsilon = 0.00075$ as in our single star model with $M = 1.35\,M_\odot$ in §3. It results in the surface rotational velocity $v_{\rm rot} \approx 10$ km s^{-1}. In fact, MS stars with $M \gtrsim 1.4\,M_\odot$ have extremely thin surface convective zones, therefore their rotation is not thought to experience magnetic braking (or other type of braking whose efficiency depends on the thickness of convective envelope). Hence, our $1.7\,M_\odot$ model should have rather been assigned $v_{\rm rot} \approx 100$ km s^{-1} instead of 10 km s^{-1}, and it should have rotated as the solid body. However, this inconsistency does not matter when we study the evolution of this model star as a primary in a close binary system because, after having been synchronized with its orbital rotation on the RGB, the primary will acquire a surface rotational velocity by far exceeding that it would have if it were a single star. So, the information about its previous surface rotation will be completely lost. What really matters is that our differentially rotating ZAMS model has approximately the same value of Ω within its inner region, that will be occupied by the radiative zone on the upper RGB, that it would have if it rotated as a solid body with $v_{\rm rot} \approx 100$ km s^{-1}. Indeed, in Fig. 10 *long-dashed horizontal line* shows the uniform rotation profile with $v_{\rm rot} \approx 100$ km s^{-1}, while *dot-long-dashed curve* presents the Ω–profile obtained using equation (5) with $f_\varepsilon = 0.00075$. Both profiles almost coincide at $M_r < 0.4\,M_\odot$. Therefore, under the assumption of the conservation of the specific angular momentum j in each mass shell, including convective regions, radiative zones of the single RGB models that have started their evolution on the ZAMS with these two different rotation profiles (the uniform one with $v_{\rm rot} \approx 100$ km s^{-1}, and the differential one with $v_{\rm rot} \approx 10$ km s^{-1}) will possess similar differential rotation. *Dot-short-dashed curve* in Fig. 10 demonstrates the rotation profile in the bump luminosity model obtained from the initial dot-long-dashed profile assuming

---

[5]According to Kippenhahn & Thomas (1970), within a high accuracy the structural changes of stars in tidally locked binaries are caused by their rotation and not by tidal forces. Therefore, we do not take into account the tidal effects on the primary's structure and evolution.

$j(t, M_r) = j(0, M_r)$ for $0 \leq M_r \leq M$. For comparison, *short-dashed horizontal line* gives the uniform Ω–profile resulted from the initial long-dashed one assuming the solid-body rotation of the whole star during its entire evolution. In all the cases, the total angular momentum is conserved. Since the bulk of the red giant's angular momentum is contained in its convective envelope, the short-dashed line also approximates quite well the envelope rotation (on the right of *vertical dotted line*) in the alternative case, that we did not consider, in which j is only conserved in radiative regions, while Ω is maintained constant in convective regions. In that case, as we mentioned, the radiative zone would rotate much slower than in the case represented by the dot-short-dashed curve (compare the values of Ω on the short-dashed and dot-short-dashed profiles at the BCE).

Before "placing" our models into binary systems, we have computed their single stellar evolution. For the metal-poor model ($M = 0.85\,M_\odot$, $Z = 0.0005$), the initial internal Ω–profile has been specified by the same parameter $f_\varepsilon = 0.0003$ as in §3. During the single stellar evolution computations, we were tabulating the quantities R, k and r_{g} as functions of age and luminosity. On the RGB, the ratio k/r_{g}^2 has been found to decrease very slightly, from about 0.5 to nearly 0.2 for both models. Hence, from equations (7) and (9) we can estimate the primary's synchronization time (the time after which $\Omega \approx \omega$) as

$$t_{\mathrm{syn}} \approx \frac{t_{\mathrm{F}}}{q^2} \left(\frac{a}{R}\right)^6 \approx 0.4304 \left[\frac{(M/M_\odot)(R/R_\odot)^2}{(L/L_\odot)}\right]^{1/3} q^{-2} \left(\frac{a}{R}\right)^6 \ \mathrm{yr}. \tag{12}$$

Furthermore, for values of $q \gtrsim 0.5$, the product in front of the last term in equation (12) does not deviate much from unity during the entire evolution of our models from the subgiant branch to the RGB tip. Therefore, for binaries with the mass ratio $0.5 \lesssim q < 1$, one can use the simpler estimate $t_{\mathrm{syn}} \approx (a/R)^6\,\mathrm{yr}$. Since the low-mass stars spend a time of the order of 10^8 yr on the RGB, only primary stars in the binaries with $a \lesssim 20\,R$ are expected to get synchronized on this evolutionary stage. If we want our primary to be tidally spun up already on the lower RGB, where $R \lesssim 10\,R_\odot$, we should only consider the binaries with $a \lesssim 200\,R_\odot$, or, in other words, only those with $P_{\mathrm{d}} \lesssim 300$ (equation (6)).

4.1.2. *Choosing a Rotation Profile in the Convective Envelope*

Unfortunately, we do not know how rotation, convection and tidal friction interact with each other in the red giant's envelope. Even 3D-hydrodynamical simulations will hardly be able to model such complex situation with confidence in the nearest future. Therefore, we cannot do anything else but to make some plausible assumptions about the outcome of this interaction and to use as many as possible relevant observational data to constrain our

assumptions. We should also choose rotation profiles and parameters of extra mixing in our binary red giant models consistent with those employed in §3 for the single star case.

In Fig. 11, we have plotted Ω–profiles in our solar-metallicity $1.7\,M_\odot$ lower RGB models that started their evolution (on the ZAMS), either as a single or a binary star, with the same rotation parameter $f_\varepsilon = 0.00075$, and so with the same value of $v_{\rm rot}$, but for which different assumptions about the rotation law in their convective envelopes were made. All the models except that plotted with *short-dashed curve* have reached nearly the same evolutionary point immediately below the bump luminosity. *Dot-dashed curve* gives the Ω–profile in the single star model. *Long-dashed, solid* and *short-dashed curves* show internal rotation of red giants in binaries with the same initial parameters: $q = 0.5$, $a = 80\,R_\odot$. *Dotted curve* has $q = 0.5$ and $a = 50\,R_\odot$.

The long-dashed curve is obtained under the assumption that, after the corotation has been achieved ($\Omega = \omega$) as a result of tidal interaction in the close binary, the whole convective envelope of the red giant rotates as the solid body, i.e. $\Omega(r) = \omega$ for $R_{\rm BCE} \leq r \leq R$. However, in this case the radiative zone would rotate slower than in the single star case (compare the parts of the dot-dashed and long-dashed curves just beneath the BCE, at $\log R/R_\odot \lesssim -0.2$). Given that on the RGB hydrogen rich material is slowly moving from the convective envelope to the helium core through the radiative zone and the specific angular momentum is assumed to be conserved in this zone, we anticipate that, in the more evolved models, the Ω–profile developed from that represented by the long-dashed curve will be parallel to the dot-dashed curve (like the short-dashed curve showing the advanced evolution of the solid curve) but it will entirely lie below it. In that case, since we assume that $D_{\rm mix} \propto \Omega^2$ (e.g., equation (1)), the rate of extra mixing would be reduced compared to the canonical case, in spite of the red giant's faster surface rotation. This seems to be at odds with the reported very high percentage of Li-rich giants among rapidly rotating stars (Drake et al. 2002) and the necessity to enhance $D_{\rm mix}$ from $\sim 10^9$ cm^2 s^{-1} to $\sim 10^{11}$ cm^2 s^{-1} in order to enable the ^{7}Be-mechanism (Denissenkov & Herwig 2004). Therefore, we reject the Ω–profile represented by the long-dashed curve as implausible.

In §3, we have made the assumption that even convective envelopes of single stars rotate differentially, with the specific angular momentum conserved in each mass shell inside them, during the entire evolution from the ZAMS. Without that assumption rotational mixing driven by the secular shear instability in the radiative zones of upper RGB stars would be too weak to be identified with canonical extra mixing. At the same time, we admit that tidal interaction in a close binary system with a red giant component can enforce solid-body rotation of at least an outer part of its convective envelope. Making an appeal to observational data, we first notice that some of the chromospherically active late-type giants

in the RS CVn binaries (for instance, those shown as *filled circles* in Fig. 9) have almost equal orbital and rotational periods. This means that their surface layers have already been spun up by the tidal drag force to the orbital angular velocity, $\Omega(R) = \omega$. Although we know nothing about their internal rotation in the convective envelope below the surface, it is naturally to think that the same tidal force induces corotation of their subsurface convective layers as well, at least down to some depth R_{cor}, i.e. $\Omega(r) = \omega$ for $R_{\mathrm{cor}} \leq r \leq R$, where $R_{\mathrm{BCE}} < R_{\mathrm{cor}} < R$. We have seen that the assumption of $R_{\mathrm{cor}} = R_{\mathrm{BCE}}$ (long-dashed curve in Fig. 11) appears to be wrong if we want to explain canonical extra mixing and the phenomenon of Li-rich giants assuming that $D_{\mathrm{mix}} \propto \Omega^2$ in both cases.

The idea that $R_{\mathrm{cor}} = R$ while $j = \mathrm{constant}$ in the convective envelope is not good either because in that case rotation of the red giant's radiative zone near the HBS $\Omega(R_{\mathrm{c}})$ could easily become supercritical. Indeed, if in the whole radiative zone $j = \mathrm{constant}$ as well, then

$$\frac{\varepsilon(r)}{\varepsilon_{\mathrm{crit}}} \approx 7.3 \times 10^{-4} \frac{(R/R_\odot)^2 (v_{\mathrm{rot}}/10\,\mathrm{km\,s^{-1}})^2}{(M_r/M_\odot)(r/R_\odot)}. \tag{13}$$

The hydrogen burning shell always stays at $r \approx R_{\mathrm{c}} \approx 0.02\,R_\odot$, and the helium core mass in stars located close to the bump luminosity is $M_r \approx 0.3\,M_\odot$, which results in $\varepsilon(r)/\varepsilon_{\mathrm{crit}} \approx 0.12\,(R/R_\odot)^2 (v_{\mathrm{rot}}/10\,\mathrm{km\,s^{-1}})^2$. Thus, in a binary RGB star that has reached a corotation at the surface with $v_{\mathrm{rot}} = 10\,\mathrm{km\,s^{-1}}$ (Fig. 3 shows that this velocity is still less than the maximum possible value), rotation near the HBS could become critical already for $R \approx 2.9\,R_\odot$, i.e. far below the bump luminosity. This disagrees with the presence of corotating binary red giants close to and even above the bump luminosity.

Equations $(7-8)$ were derived assuming for simplicity that $\Omega = \mathrm{constant}$ throughout the convective envelope. This may be a good assumption for thin convective envelopes but an RGB star has a very thick convective envelope with $R/R_{\mathrm{BCE}} \gg 1$. We can divide it into a number of thin spherical layers and consider them as rotating independently of one another. This approach is consistent with the assumption of differentially rotating convective envelopes made for single giants. If the tidal drag force had not varied along the radius inside the convective envelope then it would have naturally been to think that all the layers get synchronized at the same time. However, the transverse component of the tidal force strongly depends on r (Hut 1981),

$$F_\theta = 3\,MR\frac{k}{t_{\mathrm{F}}}q^2\left(\frac{r}{a}\right)^7(\Omega - \omega). \tag{14}$$

Therefore, the deeper convective layers are most likely to get synchronized much later than the layers near the surface.

In our work, Ω–profiles in convective envelopes of RGB model stars in close binary systems are computed as follows: *(i)* using the values of R, k and r_{g} tabulated as functions

of age and luminosity during the computations of the single stellar evolution, we first solve equations (7–8) for a specified set of parameters q and a; this gives us dependences of $v_{\rm rot}$ on L (or M_V), and Ω/ω on R, like those plotted in Figs. 12 and 13 for our solar metallicity $1.7\,M_\odot$ model in a binary system with the mass ratio $q = 0.5$ (*dashed curves* are obtained for $a = 50\,R_\odot$ ($P \approx 25$ days) while *solid curves* are for $a = 80\,R_\odot$ ($P \approx 50$ days); in Fig. 12, *solid* and *dashed curves* are computed (i.e. equations (7–8) are solved) starting with a subgiant model that has $R = 3\,R_\odot$, assuming that initially $\Omega = 0$, while *dot-dashed* and *dotted curves* — for $\Omega = 2.5 \times 10^{-5}\,{\rm rad\,s^{-1}}$ (this value of Ω extrapolates to $v_{\rm rot} \approx 100$ km s^{-1} back on the ZAMS); *(ii)* from Fig. 13, we can read the star's radius $R_{\rm cor}$ at which $\Omega/\omega = 0.9$; for the sake of simplicity, we assume that precisely at the moment when $R = R_{\rm cor}$ the star's surface comes to corotation with the binary orbital motion; we find that $R_{\rm cor} \approx 3.9\,R_\odot$ and $R_{\rm cor} \approx 6.7\,R_\odot$ for $a = 50\,R_\odot$ and $a = 80\,R_\odot$, respectively (Fig. 13); *(iii)* now, we "place" our model star into a binary system; until the star's radius $R < R_{\rm cor}$, its evolution is not considered to differ from the single star case, in particular, the whole star including its convective envelope is assumed to rotate differentially with $j(t, M_r) = j(0, M_r)$; however, as soon as $R \geq R_{\rm cor}$, the solid body rotation $\Omega(r) = \omega$ of the outer part of the convective envelope, in which $R_{\rm cor} \leq r \leq R$, is enforced.

Our algorithm can create a faster rotating radiative zone in a red giant component of a wider binary in spite of the fact that a closer binary has a higher surface rotational velocity (compare *solid* and *dotted* rotation profiles in Fig. 11). Indeed, if in the case of a tidally spun-up RGB star the specific angular momentum is still conserved in each mass shell with $R_{\rm c} \leq r \leq R_{\rm cor}$, then the angular velocity in the radiative zone will depend on the radius as $\Omega(r) = \omega(R_{\rm cor}/r)^2$, where

$$\omega = 6.274 \times 10^{-4} \left(\frac{M}{M_\odot}\right)^{1/2} (1+q)^{1/2} \left(\frac{a}{R_\odot}\right)^{-3/2}, \ {\rm rad\ s^{-1}}. \tag{15}$$

Using this equation, for our solar metallicity red giant model in the binaries with $a = 50\,R_\odot$ and $a = 80\,R_\odot$ we find $\omega_1 = 0.2834$ ($R_{\rm cor} = 3.9\,R_\odot$) and $\omega_2 = 0.1400$ ($R_{\rm cor} = 6.7\,R_\odot$), respectively (both velocities are expressed in units of $10^{-5}\,{\rm rad\,s^{-1}}$ and plotted in Fig. 10). Hence, at the same location in the radiative zone, the red giant in the binary with $a = 80\,R_\odot$ rotates 1.5 times as fast as the one in the binary with $a = 50\,R_\odot$, in spite of the fact that $\omega_2 < \omega_1$.

4.2. Possible Manifestations of Enhanced Extra Mixing

4.2.1. RS CVn binaries

As primary constraints on possible manifestations of enhanced extra mixing in giant components of tidally locked binaries, we have chosen the latest observational data on the CMD locations, rotational and orbital periods, rotational velocities, and surface element abundances for a sample of late-type red giants in the RS CVn binaries published by Fekel et al. (2002), Morel et al. (2004), and Fekel & Henry (2005). These red giants are chromospherically active stars whose activity is thought to be due to their tidal spinning up that assists in generating strong magnetic fields via convective dynamo. In order to be sure that all stars in the sample have achieved corotation, we select only those of them that have almost equal spin and orbital periods. Thus selected objects are shown as *filled circles* in Fig. 9. In the same figure, we have plotted evolutionary tracks for single solar-metallicity stars with masses 1.3, 1.5, 1.7, 2, and $3\,M_\odot$ (*dashed curves*). Looking at Fig. 9, one cannot help but noticing that all 8 of the selected RS CVn binaries are located on the lower RGBs. This striking photometric peculiarity has been emphasized by Morel et al. (2004). To extend the size of the sample of late-type red giants in tidally locked binaries, we have added a number of K-giants in binaries with circular orbits from Fig. 3 to our selected RS CVn systems (*open circles* in Fig. 9). We have used the Hipparcos parallaxes and Tycho magnitudes from the online catalogue `archive.ast.cam.ac.uk` to estimate the absolute magnitudes M_V of the additional stars. The data plotted in Fig. 9 show that the majority (15 out of 17) of the observed low-mass ($M \lesssim 2\,M_\odot$) binary stars, that are expected to experience extra mixing on the RGB and that are most likely to have synchronized their spin and orbital rotation, are still located on the lower RGB. We will show that this photometric peculiarity of the RS CVn and circularized binaries can be explained by rotational effects in the radiative zones of their tidally spun-up red giant components.

Solid curve in Fig. 9 is the evolutionary track of our solar-metallicity $1.7\,M_\odot$ model placed into a binary system with $q = 0.5$ and $a = 80\,R_\odot$. As explained before, until the model's radius R stays below the corotation radius $R_{\rm cor} = 6.7\,R_\odot$ (for $M_V \lesssim 1.68$ on the RGB), its evolution is not considered to differ from that of the single star. In particular, the surface rotational velocity $v_{\rm rot}$ decreases in a way similar to that depicted by the dot-short-dashed curve in Fig. 6. However, as soon as R exceeds $R_{\rm cor}$, the outer part of the model's convective envelope, at $R_{\rm cor} \leq r \leq R$, is enforced to rotate like the solid body with the respective orbital velocity $\Omega(r) = \omega_2$ (see Fig. 10). It means that from the moment when R becomes equal $R_{\rm cor}$ on the RGB ($M_V \approx 1.68$) the surface rotational velocity $v_{\rm rot}$ of our model starts to increase following the thin solid curve in Fig. 12. After this moment, while the surface angular velocity of our binary model's single counterpart continues to decrease

due to the conservation of the total angular momentum and the red giant's expansion, the outer convective layers of our binary model keep rotating at the same angular velocity ω_2 and its surface rotational velocity $v_{\rm rot} = R\,\omega_2$ increases with R. By the bump luminosity, the ratio of ω_2 to $\Omega(R)$ for the single model grows up to ~ 10 (compare the dot-dashed and solid curves at the maximum r in Fig. 11). At the BCE, this ratio is somewhat smaller because in the convective envelope of the single model $\Omega(r)$ increases with decreasing r all the way from R to $R_{\rm BCE}$, while in the binary model $\Omega(r)$ is maintained equal to ω_2 from the surface down to the depth $R_{\rm cor}$. Beneath the BCE, the same difference between the angular velocities for the binary and single star case that has been settled at the BCE is slowly propagating through the radiative zone, like a wave, during the subsequent stellar evolution (see the solid and short-dashed curves in Fig. 11).

Usually, when the HBS crosses the chemical composition discontinuity left behind by the BCE at the end of the first dredge-up, a low-mass star makes a tiny zigzag on the CMD, like that outlined by a small square in Fig. 4. However, in our case of the solar-metallicity $1.7\,M_\odot$ binary star the zigzag is found to be unusually big (the solid curve between $M_V \approx 0.7$ and $M_V \approx 1.5$ in Fig. 9). This is a new result which is entirely due to rotational effects. Indeed, in panel a in Fig. 14 the corotation radius is varied from 2 to $8\,R_\odot$, thus accelerating rotation of the radiative zone in the bump luminosity model of our $1.7\,M_\odot$ binary star, while panel b demonstrates how the zigzag's extent responds to the variations of $R_{\rm cor}$. These test computations have been done without extra mixing, just with rotational effects on the stellar structure and evolution included according to Denissenkov & VandenBerg (2003b). The region in the CMD in which our binary star makes the zigzag is comparable by its size with the area occupied by the majority of the observed tidally locked binaries (Fig. 9). Therefore, we surmise that it is the extended bump luminosity zigzags produced by tidal spinning up of the convective envelopes and underlying radiative zones that are responsible for the fact that the late-type giant components of the synchronized binaries predominantly reside on the lower RGB. This hypothesis receives a further support if we compare the evolutionary times or differential luminosity functions of the single and binary model stars in the vicinity of the bump luminosity. Whereas the time spent by the single star (*thick curve* in Fig. 15) between $M_V = 2$ and $M_V = 0$ is 109 million years, it takes 146 million years for the binary star (*thin curve* in Fig. 15) to make the zigzag on the CMD when its magnitude M_V first increases from 0.7 to 1.5 and then decreases back to 0.7. Besides, the bump luminosity itself is shifted by $\Delta M_V \approx 0.8$ towards the subgiant branch in the binary star case, which might explain the fact that the low-mass red giants in tidally locked binaries "prefer" to reside on the lower RGB.

For 7 out of our 8 selected RS CVn binaries, measured values of $v \sin i$ are available in the cited papers. 4 binaries have orbital periods close to 50 days, for the rest 3 of them

$P \approx 25$ days. In most cases, an estimated mass of the primary component lies between 1.5 and 1.7 $M_\odot$, and its metallicity $-0.09 \leq [\text{Fe/H}] \leq 0.12$. That is why we have chosen the solar-metallicity 1.7 $M_\odot$ model star placed in binaries with $a = 50\,R_\odot$ ($P_\text{d} \approx 25$) and $a = 80\,R_\odot$ ($P_\text{d} \approx 50$) as one of our basic binary models. Note that for $P_\text{d} = 25$ and $P_\text{d} = 50$, our binary 1.7 $M_\odot$ model with $q = 0.5$ will start to transfer matter to its companion by Roche-lobe overflow at $M_V \approx -0.03$ and $M_V \approx -0.65$, respectively, i.e. well above the observed location of the RS CVn binaries in the CMD (Fig. 9). Therefore, their scarcity on upper RGBs can hardly be attributed to a dissipation of their envelopes on a short (dynamical) timescale in a common envelope event that follows the Roche-lobe overflow. Fig. 12 shows that, within observational errors, our solutions of equations $(7-8)$, that control the tidal evolution of the red giant's angular velocity and the binary's semi-major axis, conform with the observed locations of the selected RS CVn binaries on the M_V versus $v \sin i$ plane.

The tidal spin-up of the radiative zone may transform extra mixing from its canonical to an enhanced mode, with the mixing depth and rate increased proportionally to Ω^2 according to equations $(3-4)$. *Dot-dashed curves* in panels b and d in Fig. 16 demonstrate how the diffusion coefficient D_v from equation (1) with $f_\text{v} = 1$ changes when the envelope material spun up by the tidal force eventually arrives at the HBS in our 1.7 $M_\odot$ upper RGB[6] binary model. Comparing panels c and d, we find that the tidally enforced enhanced extra mixing can dredge up some fresh Na that is being synthesized from ^{22}Ne in the HBS. This finding is not surprising because it has already been predicted for spun-up upper RGB stars by Denissenkov & VandenBerg (2003a). What is really surprising is that Na overabundances of the right magnitude have recently been reported in 5 out of our 8 selected RS CVn binaries by Morel et al. (2004). These are plotted in Fig. 17 against the Li abundances measured by the same authors. They have applied NLTE corrections to both [Na/Fe] and $\log \varepsilon(^7\text{Li})$. They have also claimed that "chromospheric heating appears insufficient to account for the anomalously high Na abundances".

We have included the effect of tidal spin-up on D_v in our stellar evolution computations. The resulting enhanced extra mixing produces *dashed curve* in Fig. 17. This curve corresponds to the stellar evolution that starts at the bump luminosity, includes the rotationally extended zigzag along the lower RGB and ends well above the bump luminosity. However, since most of the tidally synchronized binary red giants (including all 8 of our selected RS CVn binaries) in Fig. 9 are still located in the zigzag region, only the part of the dashed curve that corresponds to the evolution before the end of the zigzag should be compared with the

---

[6]We still call "the upper RGB models" those spun-up binary red giants in which the HBS has erased the composition discontinuity left behind by the BCE at the end of the first dredge-up in spite of the fact that they can reside on the lower RGB for quite a long time thereafter.

observational data points (a region between *dotted line segments* in Fig. 17). By the end of this part, [Na/Fe] reaches 0.36 and $\log\varepsilon(^7\mathrm{Li})$ accumulates only -0.6 after its initial drop by more than 3 orders of magnitude. These values are smaller than the observed abundances.

A much better result (*solid curve* in Fig. 17) is obtained with the constant diffusion coefficient $D_{\mathrm{mix}} = 10^{11}$ cm^2 s^{-1} (*dotted curve* in panel d in Fig. 16). In this case, we have actually made three simplifying assumptions: *(i)* that canonical extra mixing has operated with the constant diffusion coefficient $D_{\mathrm{mix}} = 10^9$ cm^2 s^{-1} (*dotted curve* in panel b in Fig. 16), which is close to the semi-empirical values estimated by Denissenkov & VandenBerg (2003a); *(ii)* the tidal synchronization of our binary red giant model has increased Ω in its radiative zone exactly by the factor of 10, which is even slightly less than the ratio between the Ω-profiles for the binary and single star case seen in Fig. 11; *(iii)* like D_{mix} from equation (3), our uniform diffusion coefficient scales as $D_{\mathrm{mix}} \propto \Omega^2$. It is important to note that, notwithstanding these approximations, the mixing depth has yet been determined by equation (4) because we believe firmly that it is constrained by the kinetic energy available from differential rotation of the radiative zone.

The difference between the dashed and solid curve in Fig. 17 is mainly due to the behaviour of the Li abundance, which can be explained by the same reason why $\log\varepsilon(^7\mathrm{Li})$ changes differently in a single star on the upper RGB towards the RGB tip in the secular shear instability and simple diffusion model of canonical extra mixing (compare upper panels in our Fig. 2 and in Fig. 4 from Denissenkov & VandenBerg (2003a)). In the first case, D_{mix} is proportional to the thermal diffusivity K (equation (3)) that strongly decreases with the luminosity when our tidally spun-up red giant descends along the extended bump luminosity zigzag (*solid curve* in Fig. 9). Thus, on the one hand, the tidal spinning up tends to enhance D_{mix} because $D_{\mathrm{mix}} \propto \Omega^2$ but, on the other hand, the effect of fast rotation on the red giant's internal structure causes its luminosity, and hence the value of K in the radiative zone, to drop, so the resulting mixing rate $D_{\mathrm{mix}} \propto \Omega^2 K$ turns out to be too slow, compared to the case of constant $D_{\mathrm{mix}} = 10^{11}$ cm^2 s^{-1}, to produce and support (via the ^{7}Be-mechanism) as high Li abundance as in the RS CVn binaries (Fig. 17). Of course, if, in concordance with their apparent residence on the lower RGB (Fig. 9), the RS CVn binaries have not reached their bump luminosities yet then their surface Li abundances are in good agreement with those predicted by the standard theory for the first dredge-up (*solid curve* at [Na/Fe] < 0.05 in Fig. 17). However, in that case, RS CVn binaries would not have had as large Na overabundances as those reported by Morel et al. (2004). A spectroscopic determination of CN abundances in the giant components of the RS CVn binaries could verify our hypothesis of enhanced extra mixing in these stars. Indeed, if all the assumptions made are correct then, according to our computations, these stars should have $^{12}\mathrm{C}/^{13}\mathrm{C} \approx 3.9$, [C/Fe] ≈ -1.8 and [N/Fe] ≈ 0.63 instead of the standard post-first-dredge-up

values of $^{12}C/^{13}C \approx 25$, $[C/Fe] \approx -0.17$ and $[N/Fe] \approx 0.30$.

4.2.2. Binary Red Giants in Globular Clusters

The problem of Na overabundances in RS CVn binaries and its possible solution proposed by us may be related to the long-standing problem of star-to-star abundance variations of C, N, O, Na, Mg and Al in globular clusters. At present, there are no doubts that a sizeable component of those variations originated from hydrostatic hydrogen burning in more massive stars that had completed their lives in the past. Indeed, firstly, there are correlations between overabundances of N, Na and Al and deficits of C, O and Mg as if all of them resulted from simultaneous operation of the CNO, NeNa and MgAl cycle. Secondly, the same abundance variations that are seen in red giants are also found in subgiant and MS stars, the latter evidently having too low central temperatures to produce these variations *in situ*. Hence, some of the globular-cluster MS stars must have accreted large amounts of material (or they have entirely been formed of it) processed in H-burning that had been ejected by now extinct stars into the interstellar medium of globular clusters.

Figs. 18 and 19 give nice examples of the O–Na anticorrelation and Na–Al correlation for large samples of red giants in the globular clusters M3 (*circles*) and M13 (*triangles*) recently updated by Sneden et al. (2004). If we take $[O/Fe]_{init} = 0.3$, $[Na/Fe]_{init} = -0.2$ and $[Al/Fe]_{init} = -0.2$ as the initial abundances in those M3 and M13 MS stars that were not polluted by their more massive cluster-mates, and $[O/Fe]_{acc} = -1.0$, $[Na/Fe]_{acc} = 0.7$ and $[Al/Fe]_{acc} = 1.2$ as the most extreme abundances in the material accreted by some of the cluster MS stars then both correlations can be considered as simple mixtures of a $(1 - x)$-fraction of the material with the initial abundances and an x-fraction of the (accreted) material with the most extreme abundances (*solid curves* in Figs. 18 and 19; *thick dots* on the curves mark the values of x from 0 to 1 with the increment 0.1). So, the next question is what H-burning stars were capable of producing those extreme abundances of O, Na and Al. There are two alternative answers to this question: (1) intermediate-mass $(4 - 6\,M_\odot)$ asymptotic giant branch (AGB) stars (e.g. Ventura & D'Antona 2005), or (2) upper RGB stars that had been more massive (say, $0.9 < M/M_\odot \lesssim 2$) than the present-day globular-cluster MS turn-off stars and that had experienced enhanced extra mixing caused by their tidal spin-up in binary systems (Denissenkov & VandenBerg 2003a; Denissenkov & Weiss 2004).

Since the first alternative is not without its shortcomings (e.g., when destroying O in intermediate-mass AGB stars the (hydrogen) hot-bottom burning depletes ^{24}Mg even stronger (Denissenkov & Herwig 2003); it also keeps $[C/Fe] \gtrsim -0.5$ (Denissenkov & Weiss

2004); besides, the third dredge-up in AGB stars should increase the total abundance of C+N+O (Fenner et al. 2004); *none* of these theoretical predictions is supported by observations), the second idea is worth developing. Pursuing this goal, we have computed the evolution of the $1\,M_\odot$ star with the helium mass fraction $Y = 0.24$ and $Z = 0.0005$, which gives a metallicity [Fe/H] close to those of both M3 ([Fe/H] $= -1.57$) and M13 ([Fe/H] $= -1.54$). In order to simulate tidally enforced enhanced extra mixing, this model star has been placed into a binary system with $q = 0.3$ and $a = 50\,R_\odot$. We used the same computational method and approximations as in the case of RS CVn binaries. The initial rotation parameter was $f_\varepsilon = 0.0003$, as in our $0.85\,M_\odot$ single star model with $Z = 0.0005$, and the enhancement factor in equation (3) was $f_{\rm v} = 20$. The computed evolution of the O and Na surface abundances is shown in Fig. 18 with *dashed curve.* In order to produce enough Al (*dashed curve* in Fig. 19) we had to make the same additional assumptions as in Denissenkov & Tout (2000), namely: (1) the initial abundance of the ^{25}Mg isotope was increased to $[^{25}$Mg/Fe$]_{\rm init} = 1.2$ compared to the scaled solar ratio, and (2) the reaction ^{26}Al$^{\rm g}$(p,γ)^{27}Si was sped up by the factor of 10^3 compared to its rate from Angulo et al. (1999).

Comparing the binary red giant evolution with that of a single red giant with the same mass and composition, we have found that the tidal spin-up has accelerated rotation of the radiative zone by a factor of ~ 20. Taking into account intrinsic imperfections of our description of the tidal spin-up, we have also considered a test case in which rotation of the red giant's radiative zone has artificially been maintained 25 times as fast as in the single red giant model. For this test case, the correlated O, Na and Al abundance variations are depicted with *dotted curves* in Figs. 18 and 19. In both cases, the abundances of O, Na and Al naturally evolve from their initial values of [O/Fe]$_{\rm init} = 0.3$, [Na/Fe]$_{\rm init} = -0.2$ and [Al/Fe]$_{\rm init} = -0.2$ close to the most extreme values supposedly present in the material accreted by globular-cluster MS stars.

It is important to note that environmental conditions in globular clusters are likely to be appropriate for our binary star scenario to contribute to the star-to-star abundance variations. Firstly, frequent single-binary and binary-binary stellar encounters work toward decreasing the semi-major axes of hard binaries (Hut et al. 1992). In particular, Beer & Davies (2004) have recently shown that after ~ 20 of such encounters the initial $\log a$-flat binary population transforms into a gaussian-like distribution with a peak at $a \approx 100\,R_\odot$. Secondly, binary red giants with $a \leq 100\,R_\odot$ will definitely fill their Roche lobes before reaching the RGB tip. Therefore they will probably lose their convective envelopes very quickly during a common-envelope phase (Beer & Davies 2004). According to our hypothesis, these envelopes will be enriched with Na and Al while O will be depleted due to enhanced extra mixing triggered by their tidal spin-up. Finally, a fraction of primordial binaries in globular clusters migh have been very high, up to 100% (Ivanova et al. 2005).

5. Concluding Remarks

In this paper, we have elaborated upon the ideas proposed by Denissenkov & Vanden-Berg (2003a) about canonical extra mixing in single upper RGB stars and enhanced extra mixing in low-mass red giants spun-up as a result of their tidal synchronization in close binary systems. In order to put as many as possible observational constraints on properties of extra mixing, we have supplemented the old data on the Li and CN abundance changes along upper RGBs in field low-metallicity stars with the new data on photometry, chemical peculiarities and rotational periods/velocities of stars from the solar-metallicity open cluster M67, globular clusters 47 Tuc, NGC 6397, NGC 6752, and RS CVn binaries.

We have confirmed the conclusions made in the earlier paper that the secular shear instability driven by differential rotation of the red giants' radiative zones can be considered as a promising physical mechanism for both modes of extra mixing while the turbulent diffusion coefficient (1) derived by Maeder & Meynet (1996) can be used to model them appropriately, provided that: *(i)* unlike the Sun, low-mass MS progenitors of those red giants already possessed differentially rotating radiative cores; *(ii)* the specific angular momentum was conserved in each mass shell, including convective regions, inside those stars during their entire evolution from the MS through the RGB tip; and *(iii)* the diffusion coefficient (1) is taken with the enhancement factor $f_{\rm v} \approx 20$. For a binary red giant, we have additionally assumed that the tidal force brings to corotation only an upper part of its convective envelope. For the orbital and stellar parameters typical for the RS CVn binaries, this assumption results in spinning up of their radiative zones by a factor of $\gtrsim 10$.

Although we present some arguments in support of the made assumptions, it still seems unlikely that even our tidally enforced enhanced extra mixing with $D_{\rm mix} \sim 10^{11}$ cm^2 s^{-1} is not accompanied by a fast transport of angular momentum that would work toward flattening the Ω-profile in the radiative zone, thus reducing the mixing efficiency. From this point of view, our approach to modeling extra mixing in upper RGB stars is similar to the "Maximal Mixing Approach" recently used by Chanamé et al. (2005). The question "how far is our approach from reality?" can be answered in the usual way — by comparing the theoretical predictions made by us with future observations. Here are some possible observational tests that can support or reject our models.

First, we propose to determine ^{12}C/^{13}C ratios in upper RGB stars in the solar-metallicity open cluster NGC 6791 whose MS turn-off mass is $\sim 1.1\,M_\odot$. If the Sun is not an exceptional case then, like the Sun, MS progenitors of the NGC 6791 red giants must have rotated as solid bodies. Therefore, we expect that canonical extra mixing in upper RGB stars in NGC 6791 should be inefficient. Hence, these stars should keep their post-first-dredge-up values of ^{12}C/^{13}C ≈ 25 unchanged instead of having the values of ^{12}C/^{13}C ≈ 10 similar to

those measured in the M67 evolved stars that have definitely experienced canonical extra mixing.

Second, although we do believe that the depth of extra mixing is constrained by equation (4), when computing its rate, we still cannot choose between the constant diffusion coefficient ($D_{\mathrm{mix}} \approx 10^9$ cm^2 s^{-1} for canonical and $D_{\mathrm{mix}} \approx 10^{11}$ cm^2 s^{-1} for enhanced extra mixing) and the turbulent diffusion coefficient (3) that is proportional to the radiative diffusivity K. The first coefficient better reproduces the Na–Li data for RS CVn binaries and, unlike the second one, it actually results in a steeper decline of the ^{12}C/^{13}C ratio immediately after the bump luminosity as appears to be dictated by observations (e.g., compare the $\log {}^{12}$C/^{13}C panels in our Fig. 2 and in Fig. 4 from Denissenkov & VandenBerg (2003a)). Fortunately, one probably can discriminate between the diffusion coefficients by measuring the Li abundance in RGB tip and clump stars. As we have predicted, in the case of $D_{\mathrm{mix}} \propto K$ these evolved stars should have values of $\log \varepsilon (^7\mathrm{Li}) \gtrsim 1$ comparable with the post-first-dredge-up values or even exceeding them. Tentatively, this theoretical prediction seems to have been already confirmed by Pasquini et al. (2001). However, we think more observational work should be done in this direction.

Finally, we surmise that red giant components of the RS CVn binaries experience enhanced extra mixing caused by their tidal spin-up. We think that the large Na abundances found in these stars by Morel et al. (2004) support this idea. We did not mention before that the same authors had also reported high Al abundances in the RS CVn binaries. It is interesting that a similar Na–Al correlation commonly inheres in the star-to-star abundance variations in globular clusters. One of its possible interpretations also employs a model of tidally enforced enhanced extra mixing in a binary red giant (§ 4.2.2). If it could be possible to corroborate our hypothesis of enhanced extra mixing in the RS CVn binaries observationally that would also prove that a large amount of Al can be produced at the same physical conditions under which Na is synthesized (this actually requires higher rates for the MgAl-cycle reactions responsible for the Al production). We propose to determine ^{12}C/^{13}C ratios and/or CN abundances in the RS CVn binaries to see whether they are consistent with those resulting from enhanced extra mixing.

REFERENCES

Alexander, M. E. 1973, Ap&SS, 23, 459

Alexander, D. R., & Ferguson, J. W. 1994, ApJ, 437, 879

Angulo, C., Arnold, M., Rayet, M., Descouvemont, P., Baye, D., Leclercq-Willain, C., Coc, A., Barhoumi, S., Aguer, P., Rolfs, C., et al. 1999, NuPhA, 656, 3

Beer, M. E., & Davies, M. B. 2004, MNRAS, 348, 679

Bellman, S., Briley, M. M., Smith, G. H., & Claver, C. F. 2001, PASP, 113, 326

Brüggen, M., & Hillebrandt, W. 2001, MNRAS, 320, 73

Cassisi, S., Salaris, M., & Bono, G. 2002, ApJ, 565, 1231

Cameron, A. G. W., & Fowler, W. A. 1971, ApJ, 164, 111

Canuto, V. M. 2002, A&A, 384, 1119

Canuto, V. M., & Mazzitelli, I. 1991, ApJ, 370, 295

Chaboyer B., Green, E. M., & Liebert, J. 1999, AJ, 117, 1360

Chanamé J., Pinsonneault, M., & Terndrup, D. M. 2005, ApJ, 631, 540

Chaplin, W. J., Christensen-Dalsgaard, J., Elsworth, Y., Howe, R., Isaak, G. R., Larsen, R. M., New, R., Schou, J., Thompson, M. J., Tomczyk, S. 1999, MNRAS, 308, 405

Charbonnel, C. 1994, A&A, 282, 811

Charbonnel, C. 1995, ApJ, 453, L41

Charbonnel, C., & Balachandran, S. C. 2000, A&A, 359, 563

Charbonnel, C., Brown, J. A., & Wallerstein, G. 1998, A&A, 332, 204

Charbonnel, C., & do Nascimento, J. D. Jr. 1998, A&A, 336, 915

Claret, A., & Willems, B. 2002, A&A, 388, 518

De Medeiros, J. R., Da Silva, J. R. P., & Maia, M. R. G. 2002, ApJ, 578, 943

Denissenkov, P. A., & Tout, C. A. 2000, MNRAS, 316, 395

Denissenkov, P. A., & Weiss, A. 2000, A&A, 358, L49

Denissenkov, P. A., & VandenBerg, D. A. 2003a, ApJ, 593, 509

Denissenkov, P. A., & VandenBerg, D. A. 2003b, ApJ, 598, 1246

Denissenkov, P. A., & Herwig, F. 2003, ApJ, 590, L99

Denissenkov, P. A., & Herwig, F. 2004, ApJ, 612, 1081

Denissenkov, P. A., & Weiss, A. 2004, ApJ, 603, 119

Drake, N. A., de la Reza, R., da Silva, L., & Lambert, D. L. 2002, ApJ, 123, 2703

Eggleton, P. P. 1983, ApJ, 268, 368

Fekel, F. C., Henry, G. W., Eaton, J. A., Sperauskas, J., & Hall, D. S. 2002, AJ, 124, 1064

Fekel, F. C., & Henry, G. W. 2005, AJ, 129, 1669

Fenner, Y., Campbell, S., Karakas, A. I., Lattanzio, J. C., & Gibson, B. K. 2004, MNRAS, 353, 789

Gilroy, K. K. 1989, ApJ, 347, 835

Gilroy, K. K., & Brown, J. A. 1991, ApJ, 371, 578

Gratton, R. G., Sneden, C., Carretta, E., & Bragaglia, A. 2000, A&A, 354, 169

Grundahl, F., Briley, M., Nissen, P. E., & Feltzing, S. 2002, A&A, 385, L14

Hartoog, M. R. 1978, PASP, 90, 167

Hurley, J. R., Tout, C. A., & Pols, O. R. 2002, MNRAS, 329, 897

Hut, P. 1981, A&A, 99, 126

Hut, P., McMillan, S., & Romani, R. W. 1992, ApJ, 389, 527

Iben, I., Jr. 1967, ApJ, 147, 624

Itoh, N., Hayashi, H., Nishikawa, A., & Kohyama, Y. 1996, ApJS, 102, 411

Ivanova, N., Belczynski, K., Fregeau, J. M., & Rasio, F. A. 2005, MNRAS, 358, 572

Kippenhahn, R., & Thomas, H.-C. 1970, in IAU Coll. 4, Stellar Rotation, ed. A. Slettebak (Dordrecht: Reidel), 20

Langer, G. E., Kraft, R. P., Carbon, D. F., Friel, E., & Oke, J. B. 1986, PASP, 98, 473

Lucatello, S., & Gratton, R. G. 2003, A&A, 406, 691

Maeder, A., & Meynet, G. 1996, A&A, 313, 140

Melo, C. H. F., Pasquini, L., & De Medeiros, J. R. 2001, A&A, 375, 851

Monaco, L., Ferraro, F. R., Bellazzini, M., & Pancino, E. 2002, ApJ, 578, L47

Morel, T., Micela, G., Favata, F., & Katz, D. 2004, A&A, 426, 1007

Pasquini, L., Randich, S., & Pallavicini, R. 2001, A&A, 374, 1017

Riello, M., Cassisi, S., Piotto, G., Recio-Blanco, A., De Angeli, F., Salaris, M., Pietrinferni, A., Bono, G., & Zoccali, M. 2003, A&A, 410, 553

Rogers, F. J., & Iglesias, C. A. 1992, ApJ, 401, 361

Salaris, M., Cassisi, S., & Weiss, A. 2002, PASP, 114, 375

Sandquist, E. L. 2004, MNRAS, 347, 101

Shetrone, M. D. 2003, ApJ, 585, L45

Smith, G. H., & Tout, C. A. 1992, MNRAS, 256, 449

Smith, G. H., & Martell, S. L. 2003, PASP, 115, 1211

Sneden, C., Pilachowski, C. A., & VandenBerg, D. A. 1986, ApJ, 311, 826

Sneden, C., Kraft, R. P., Guhathakurta, P., Peterson, R. C., & Fulbright, J. P. 2005, AJ, 127, 2162

Sweigart, A. V., & Mengel, J. G. 1979, ApJ, 229, 624

Talon, S., & Charbonnel, C. 2004, A&A, 418, 1051

VandenBerg, D. A., & Smith, G. H. 1988, PASP, 100, 314

Ventura, P., & D'Antona, F. 2005, A&A, 431, 279

Zahn, J.-P. 1977, A&A, 57, 383

Zoccali, M., Cassisi, S., Piotto, G., Bono, G., & Salaris, M. 1999, ApJ, 518, L49
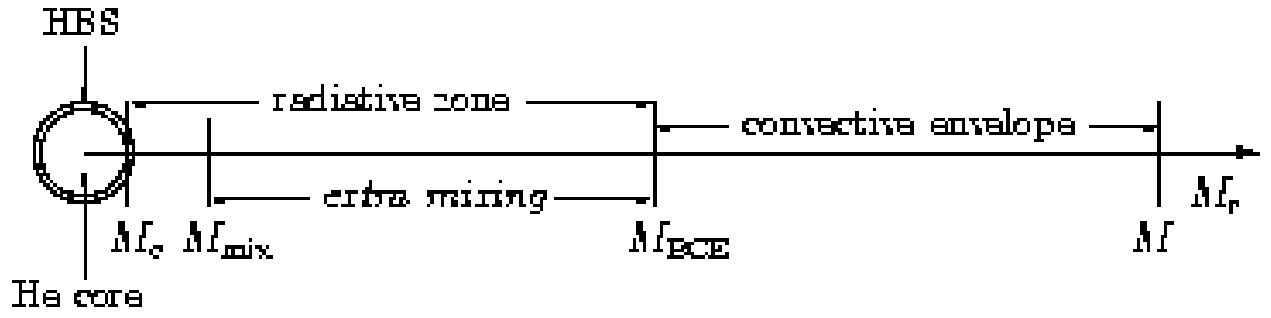
Fig. 1.— Schematic structure of a red giant with extra mixing in its radiative zone. HBS and BCE stand for the "hydrogen burning shell" and the "bottom of the convective envelope".
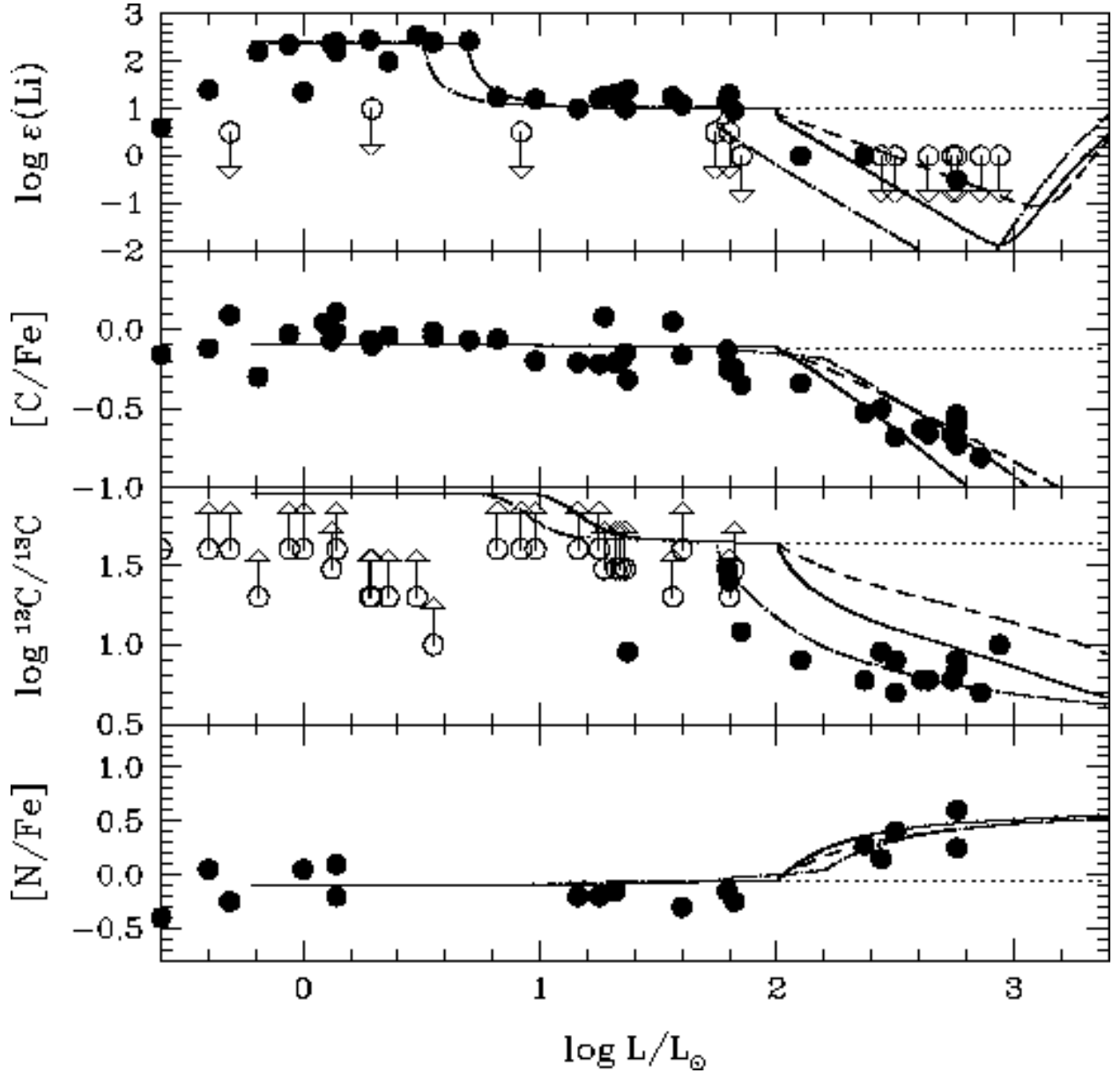
Fig. 2.— Comparison of the observational data from Gratton et al. (2000) for field metal-poor ($-2 \lesssim$ [Fe/H] $\lesssim -1$) low-mass stars (*circles*) with results of our stellar evolution computations with rotational mixing on the upper RGB described by equation (1). It is assumed that the specific angular momentum is conserved in each mass shell, including convective regions, during the entire stellar evolution. Computations are done for $M = 0.85\,M_\odot$ and the initial rotation parameter $f_\varepsilon = 0.0003$ (equation (5)). Theoretical results are presented for the following combinations of the enhancement factor (f_v in equation (1)) and heavy-element mass fraction: $f_v = 25$ for $Z = 0.0005$ and $Z = 0.002$ (*solid and dot-dashed curves*, respectively), and $f_v = 15$ for $Z = 0.0005$ (*dashed curve*).
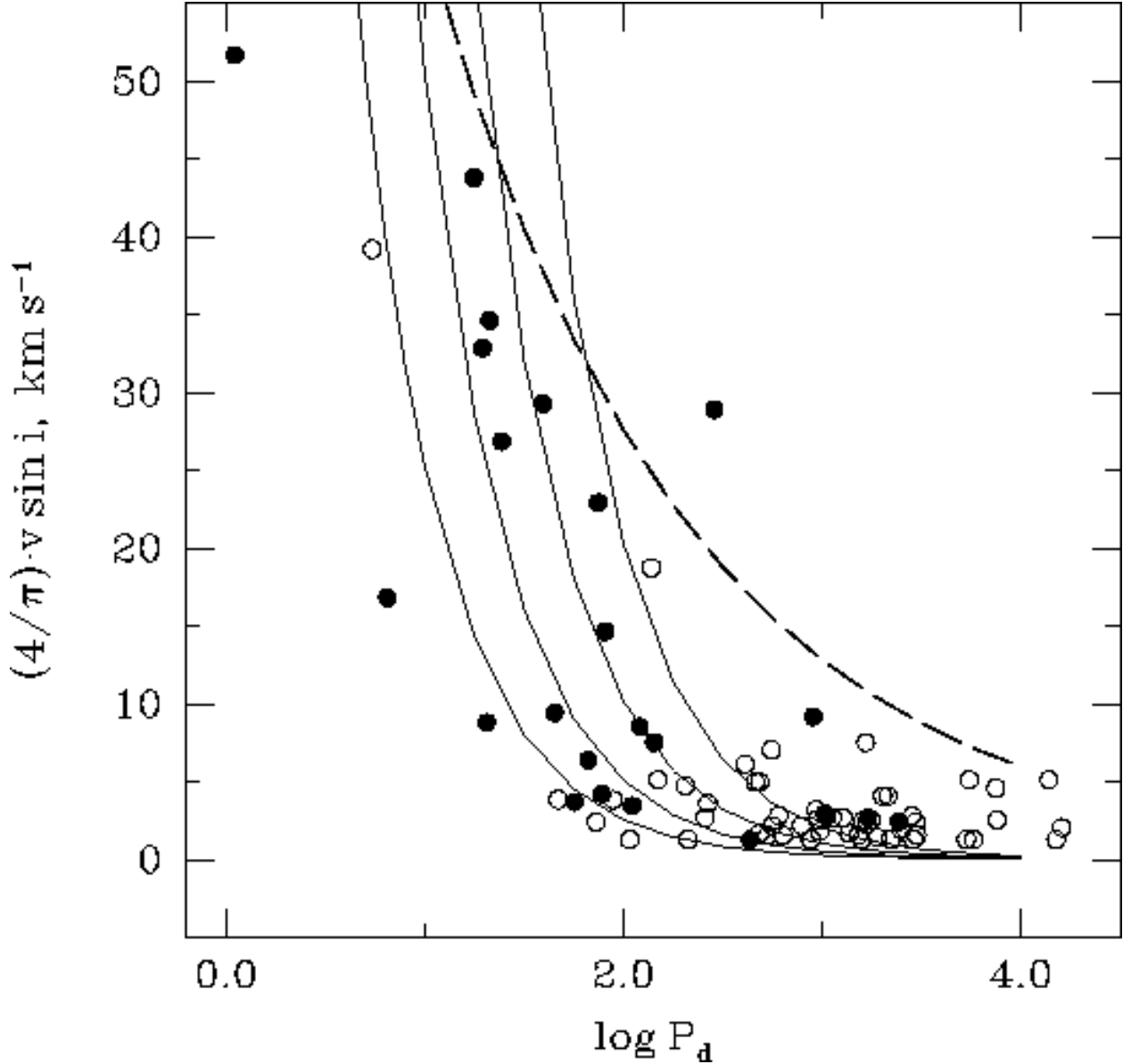
Fig. 3.— An illustration of tidal synchronization in real stars. *Circles* are G and K giant components of field binaries observed by De Medeiros et al. (2002). The factor $4/\pi \approx 1.27$ takes into account the random orientation of their rotation axes. P_d is the binary orbital period in days. *Filled circles* are binaries with nearly circular orbits (eccentricities $e \leq 0.10$). The systems with $e > 0.10$ are represented by *open circles*. A set of theoretical *solid curves* is constructed by us assuming that $\Omega = \omega$, where Ω and ω are the spin and orbital angular velocity of a red giant, for radii $R/R_\odot = 5$, 10, 20 and 40 (from left to right). The giants represented by filled circles are most likely to have synchronized their rotation. *Dashed curve* shows the maximum possible v_rot of a red giant that fills its Roche lobe in a binary system with $M = 1.7\,M_\odot$, $q = 0.5$.
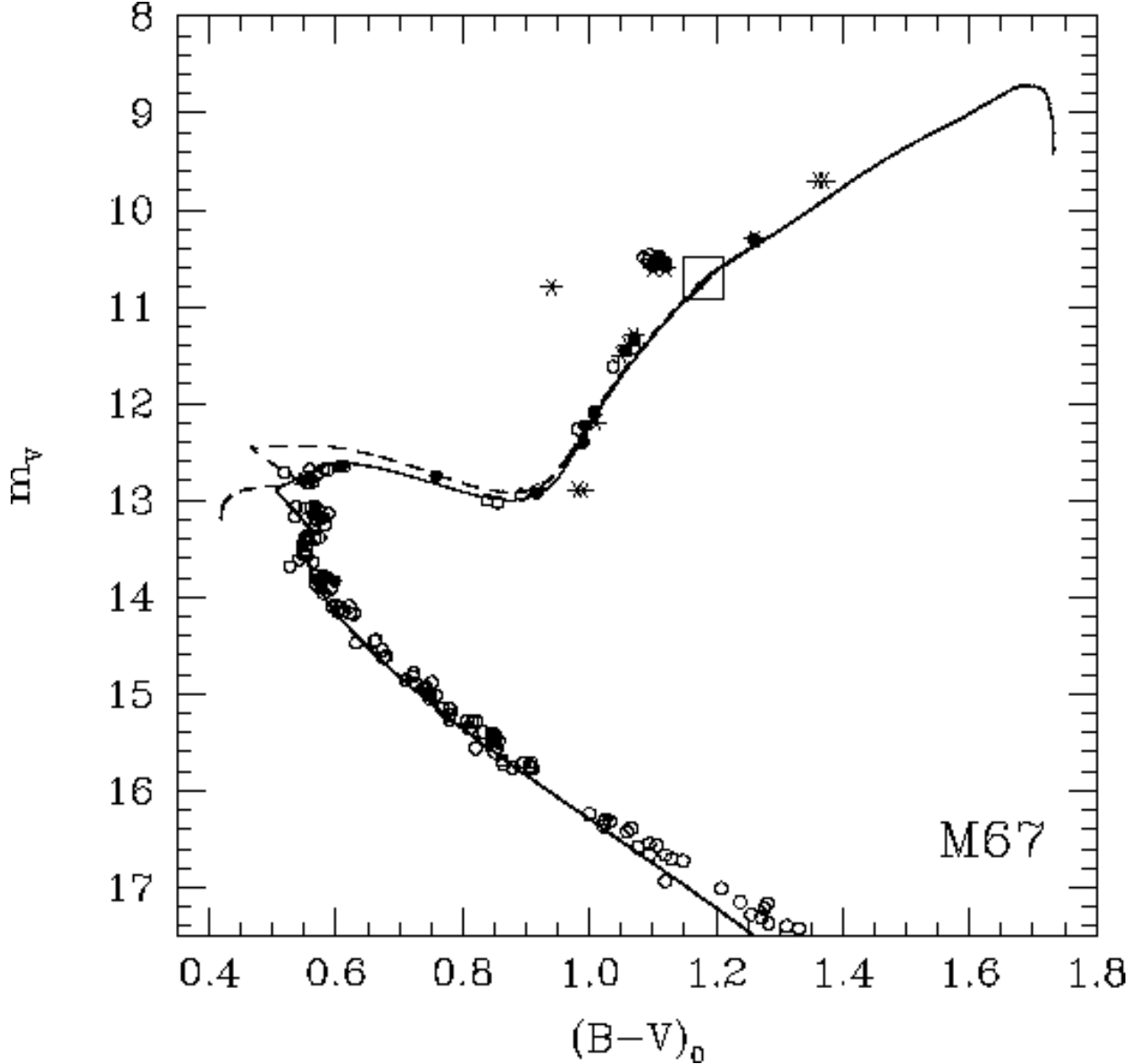
Fig. 4.— High precision CMD of the old solar-metallicity open cluster M67 (*open circles*) from the data of Sandquist (2004) and our 4×10^9 yr isochrone (*solid curve*). A region around the bump luminosity is outlined by a square. *Dashed curve* is the evolutionary track of the model star with $M = 1.35\,M_\odot$ and $Z = Z_\odot = 0.0188$. All models were computed with the same initial rotation parameter $f_\varepsilon = 0.00075$. *Filled circles* are stars with known values of $v \sin i$ from Melo et al. (2001). *Asterisks* are red giants and clump stars for which the ratio $^{12}C/^{13}C$ was measured by Gilroy & Brown (1991). For the cluster reddening and distance modulus, we have adopted the values $E(B - V) = 0.03$ and $(m - M)_V = 9.67$ that correspond to the observational lower limits provided by Sandquist (2004).
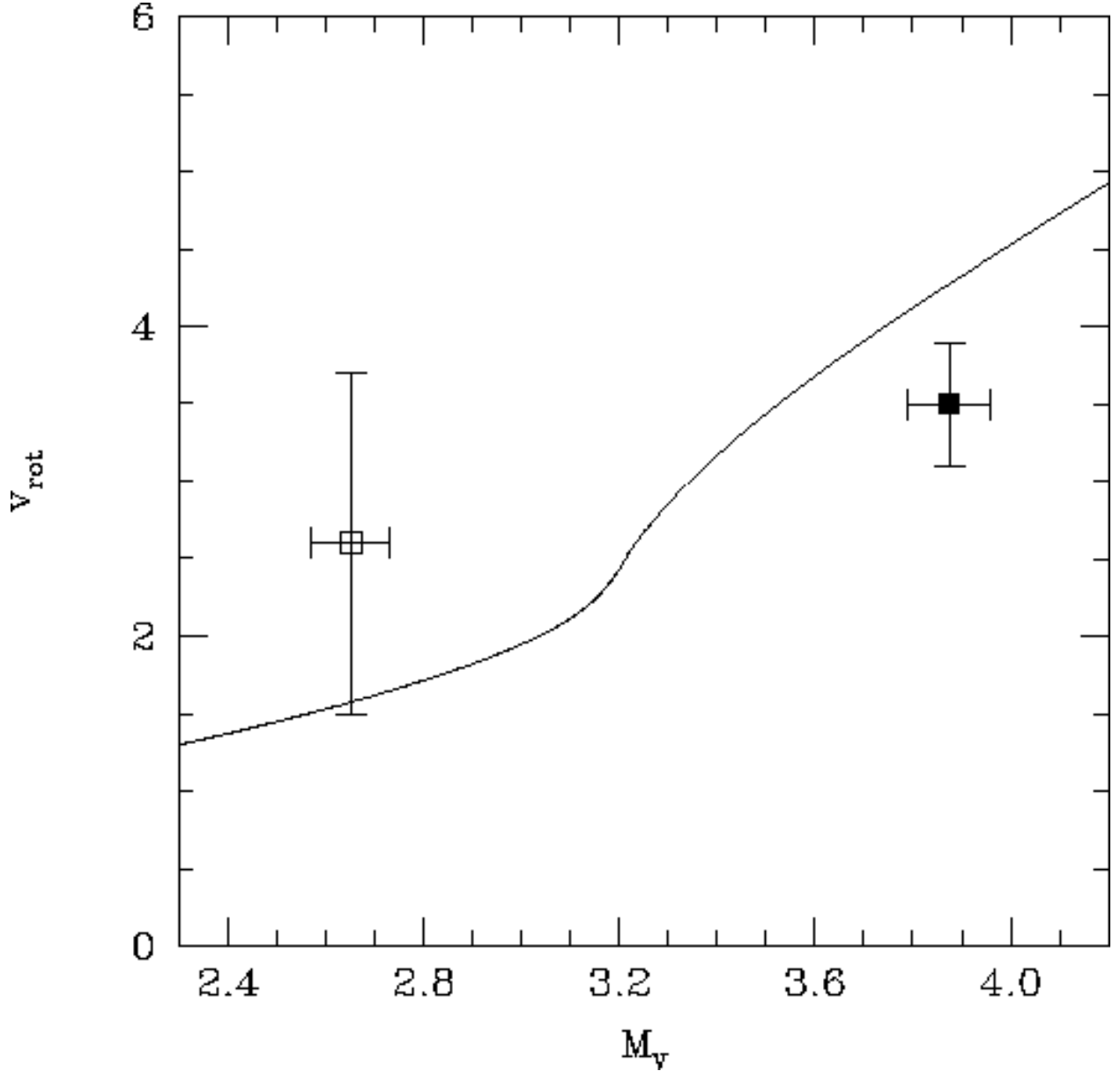
Fig. 5.— Estimates of the upper limits for the "true" mean rotational velocities of stars in globular clusters 47 Tuc, NGC 6397 and NGC 6752 by Lucatello & Gratton (2003). *Filled square* — a mean for MS turn-off stars, *open square* — for subgiants. Horizontal errorbars embrace all M_V values for the observed samples of stars in NGC 6752 ([Fe/H] $= -1.43$). Theoretical curve shows how $v_{\rm rot}$ changes during the evolution of our model star with $M = 0.85\,M_\odot$ and $Z = 0.0005$ in which the specific angular momentum is conserved in each mass shell.
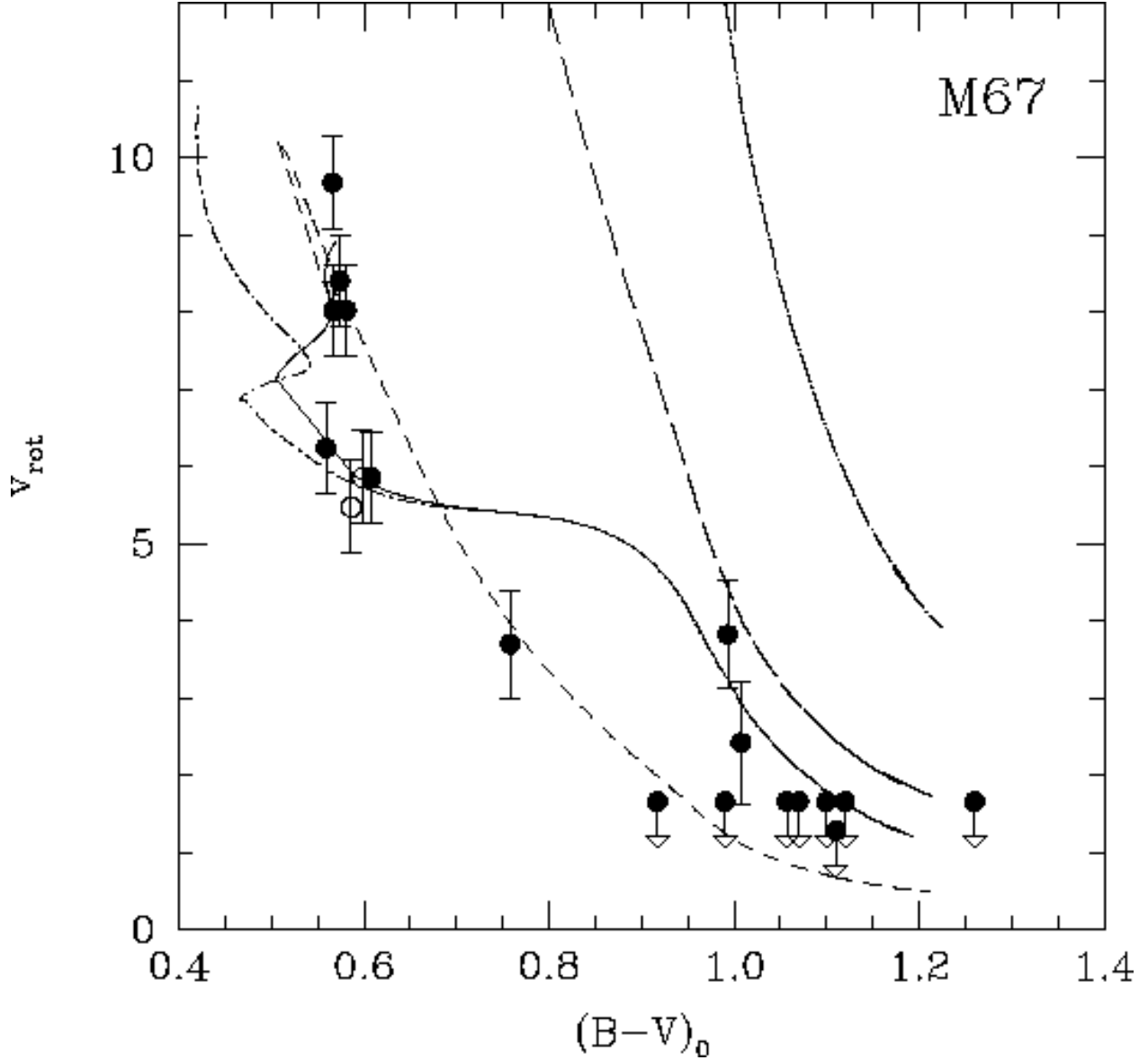
Fig. 6.— Observational data on $(4/\pi)\,v\sin i$ for M67 stars (*open circles* are MS stars, *filled circles* are MS turn-off, subgiant and lower RGB stars) from Melo et al. (2001) and theoretical dependences of $v_{\rm rot}$ on $(B-V)_0$. *Solid curve* — the 4×10^9 yr rotational isochrone for $Z = 0.0188$. *Dot-short-dashed curve* shows the rotational evolution of our $1.35\,M_\odot$ model. Both curves are computed under the assumption of constant specific angular momentum in each stellar mass shell for the initial rotation parameter $f_\varepsilon = 0.00075$. *Short-dashed curve* is the 4×10^9 yr isochrone with the initial velocity $v_{\rm rot} \approx 10$ km s^{-1} computed assuming solid-body rotation inside all of the $M \geq 1.1\,M_\odot$ models used to construct it. For comparison, *dot-long-dashed curve* and *long-dashed curve* represent the evolution of the $1.35\,M_\odot$ model for the cases of differential and solid-body rotation, respectively, but for the initial velocity $v_{\rm rot} \approx 40$ km s^{-1}.
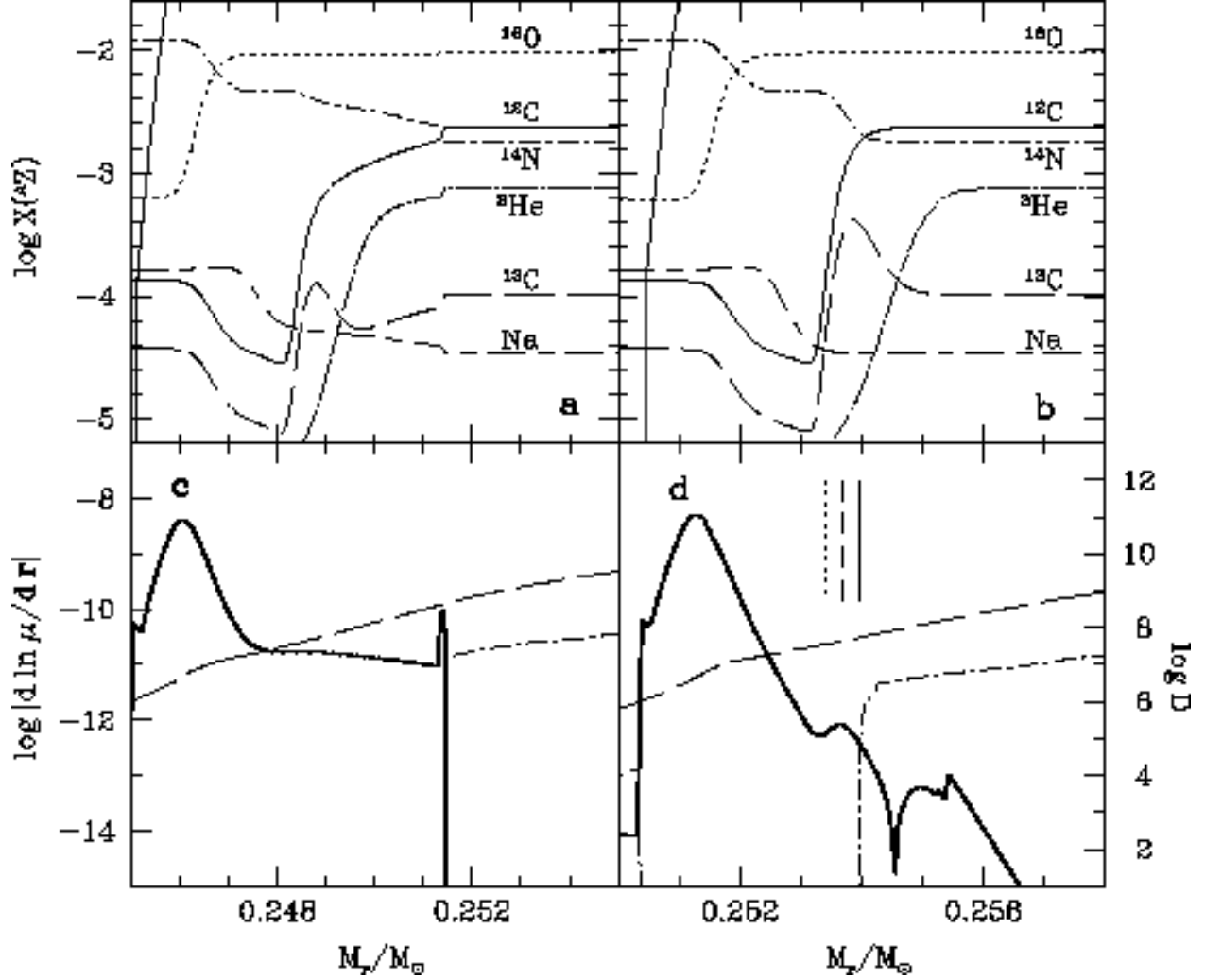
Fig. 7.— Profiles of some element abundances (mass fractions in panels a and b), μ-gradients and diffusivities (panels c and d) near the HBS in two rotating RGB models with $M = 1.35\,M_\odot$, $Z = 0.0188$ and the initial rotation parameter $f_\varepsilon = 0.00075$. The models are located immediately above (panels b and d) and below (panels a and c) the bump luminosity. In panels c and d, the μ-gradients are plotted using *solid curves*, thermal diffusivity K — *long-dashed curves*, coefficients of the vertical turbulent diffusion D_v (these are given by equation (1) for the enhancement factor $f_v = 15$) — *dot-dashed curves*. Vertical line segments in panel d point to the extra mixing depths specified by parameters $\Delta \log T = 0.19$ (*dotted line*) and $\Delta \log T = 0.22$ (*dashed line*) as well as to the depth determined by equation (4) (*solid line*).
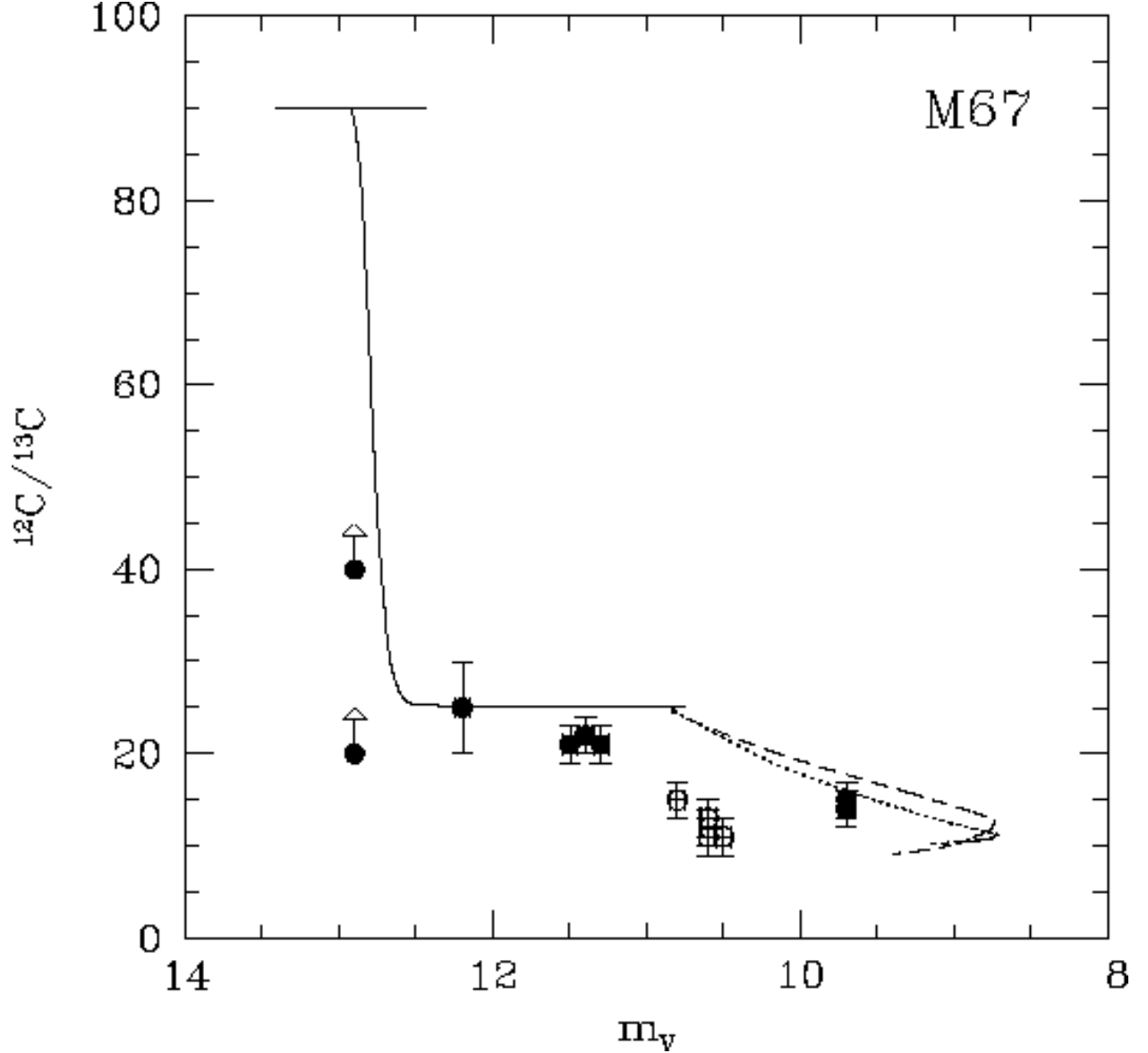
Fig. 8.— ^{12}C/^{13}C isotopic ratios in the M67 evolved stars measured by Gilroy & Brown (1991) (*symbols with arrows and errorbars*). *Filled circles* are RGB stars while *open circles* are clump stars. *Solid curve* shows a decrease of ^{12}C/^{13}C produced by the standard first dredge-up for the model star with $M = 1.35\,M_\odot$ and $Z = 0.0188$. *Dotted curve* presents results of our computations in which extra mixing on the upper RGB has been simulated using the diffusion model with the depth and rate parameters: $\Delta \log T = 0.22$ and $D_{\mathrm{mix}} = 8 \times 10^8$ cm^2 s^{-1}. *Dashed curve* is obtained for our rotating evolutionary model with extra mixing modeled by the vertical turbulent diffusion (the diffusion coefficient from equation (1) with the enhancement factor $f_{\mathrm{v}} = 15$). The initial rotation parameter was $f_\varepsilon = 0.00075$.
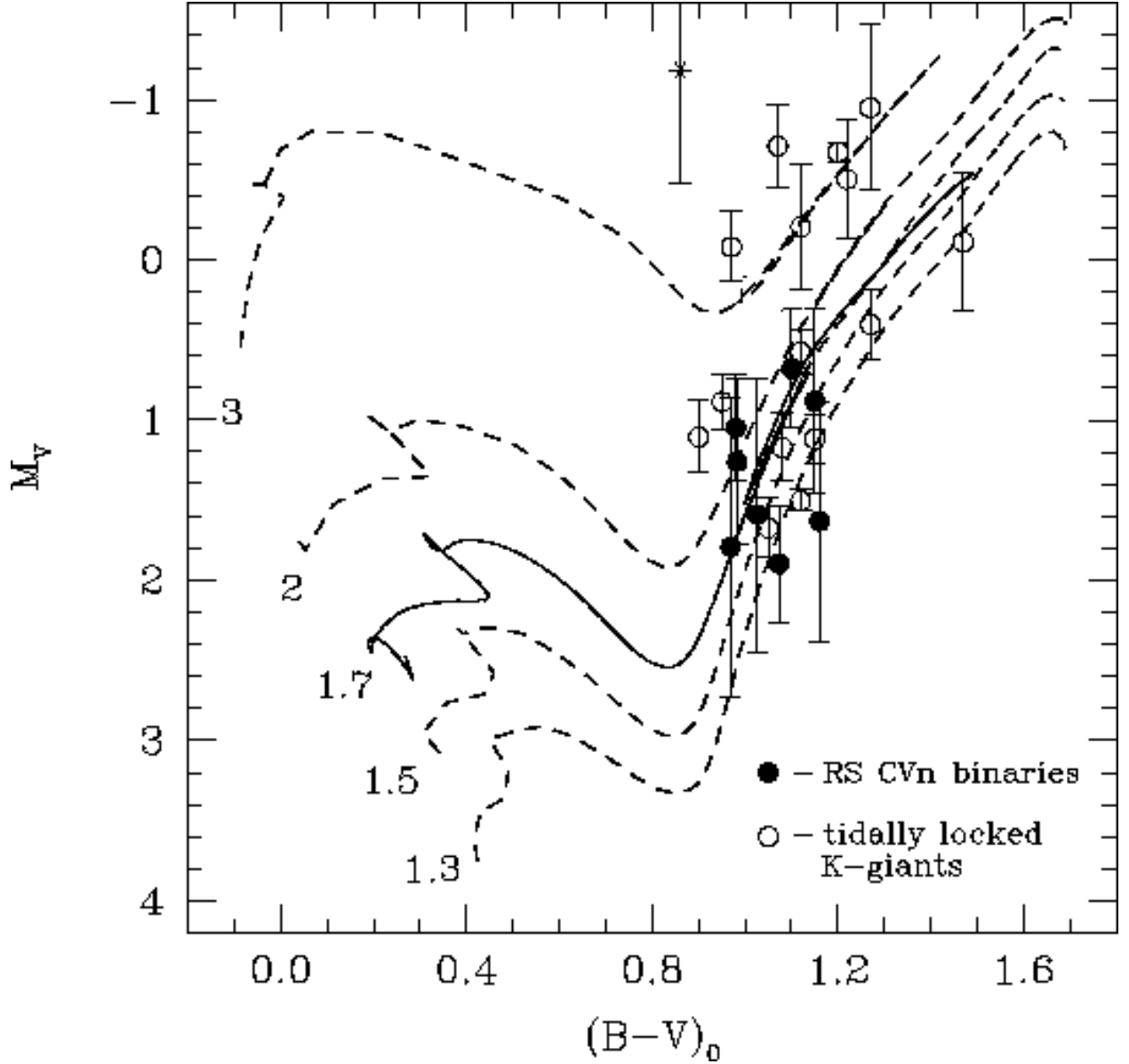
Fig. 9.— *Dashed curves* are evolutionary tracks of single solar-metallicity stars. Their masses are indicated on the left from the tracks. *Solid curve* shows the evolution of the 1.7 $M_\odot$ star placed into a binary system with $q = 0.5$ and $a = 80\,R_\odot$. Its initial rotation is specified by the parameter $f_\varepsilon = 0.00075$. After having been tidally spun up on the lower RGB, this binary star makes an extended bump luminosity zigzag between $M_V \approx 0.7$ and $M_V \approx 1.5$. *Filled circles* are RS CVn binaries that have nearly solar metallicities and estimated masses $1.5 \lesssim M/M_\odot \lesssim 1.7$ (Fekel et al. 2002; Morel et al. 2004; Fekel & Henry 2005). Each of them has almost equal rotational and orbital periods that correspond to $a \approx 50\,R_\odot$ or $a \approx 80\,R_\odot$. *Open circles* are binary red giants with circularized orbits from Fig. 3. *Asterisk* is the star HD 21018 that lies above the dashed curve in Fig. 3.
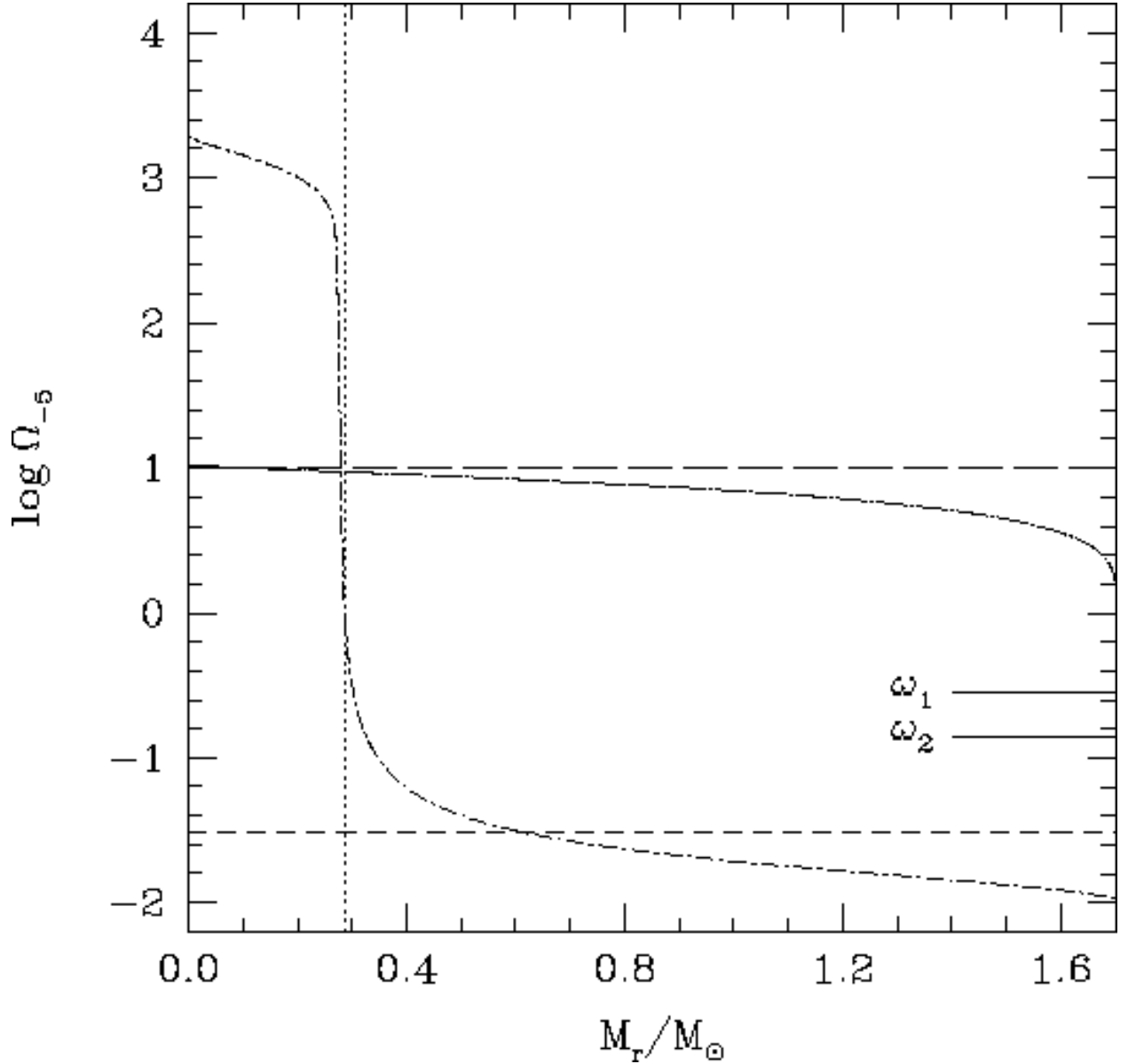
Fig. 10.— *Dot-long-dashed* and *dot-short-dashed curves* are the ZAMS and bump luminosity Ω-profiles in the single model star with $M = 1.7\,M_\odot$, $Z = 0.0188$ and initial rotation parameter $f_\varepsilon = 0.00075$ rotating differentially (with the specific angular momentum conserved in each mass shell). *Long-dashed* and *short-dashed curves* are the ZAMS and bump luminosity Ω-profiles in the same model but for the case of its evolution with uniform rotation starting on the ZAMS with $v_{\rm rot} \approx 100\ {\rm km\,s^{-1}}$. *Solid line segments* show the orbital angular velocities $\omega_1 = 0.2834$ and $\omega_2 = 0.1400$ (in units of $10^{-5}\,{\rm rad\,s^{-1}}$) for binary systems with a $1.7\,M_\odot$ primary component, the same mass ratio $q = 0.5$ but with different semi-major axes $a = 50\,R_\odot$ and $a = 80\,R_\odot$, respectively. Vertical *dotted line* marks location of the BCE in the bump luminosity models.
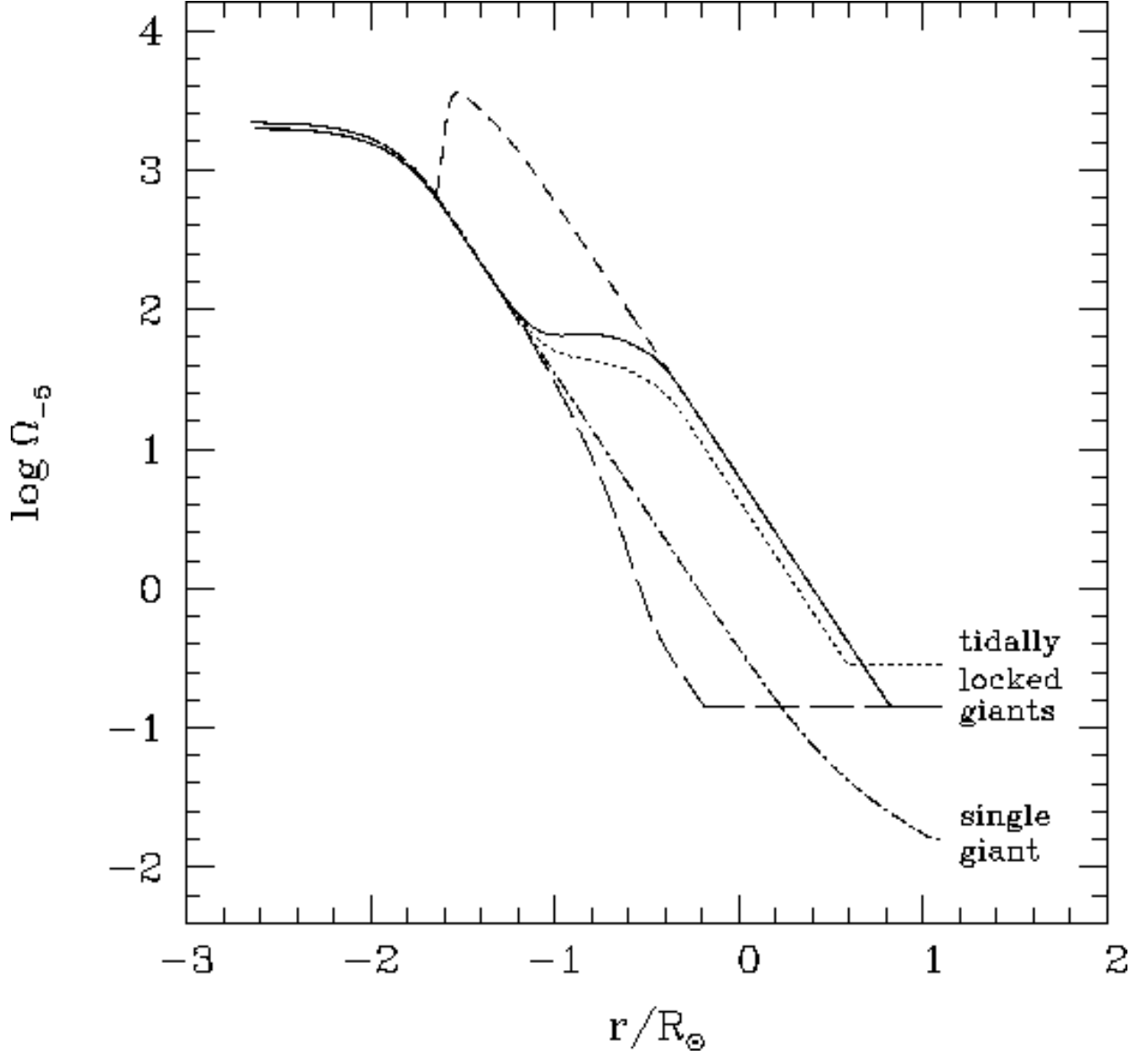
Fig. 11.— Bump luminosity and a later Ω-profiles in differentially rotating star with $M = 1.7\,M_\odot$, $Z = 0.0188$ and initial rotation parameter $f_\varepsilon = 0.00075$. *Dot-dashed curve* — in a single star. *Solid curve* — in a binary star with $q = 0.5$ and $a = 80\,R_\odot$. It is assumed that only an upper part of convective envelope is spun up by the tidal force (for details, see text). *Short-dashed curve* — a later profile evolved from the solid one. *Long-dashed curve* — in the same binary star but under the assumption that rotation of the whole convective envelope has been tidally synchronized. *Dotted curve* — a binary star with $q = 0.5$ and $a = 50\,R_\odot$.
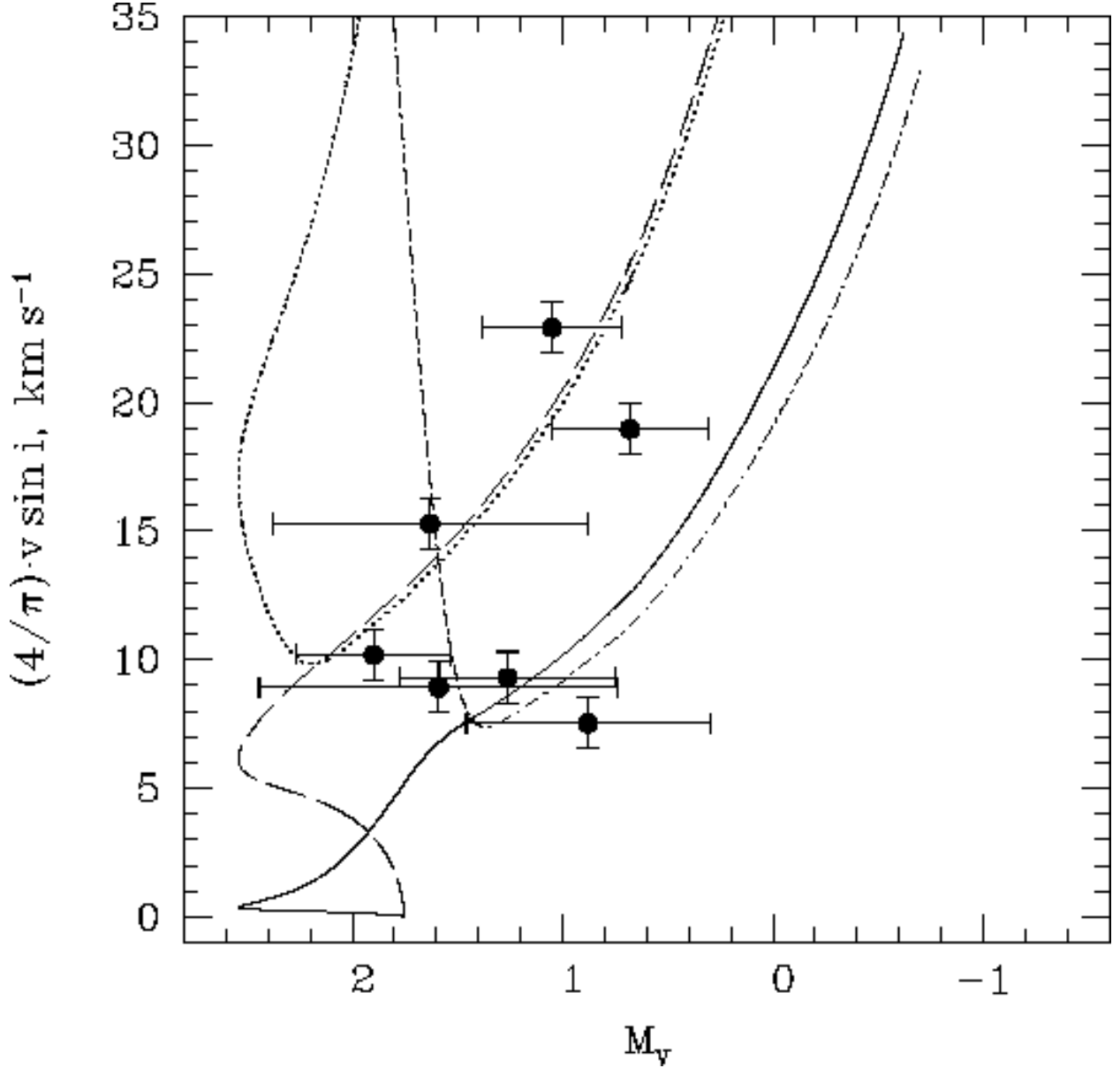
Fig. 12.— Theoretical dependences of the surface rotational velocity $v_{\rm rot}$ on M_V for the solar-metallicity $1.7\,M_\odot$ primary star in binaries with the same $q = 0.5$ but different semi-major axes: $a = 50\,R_\odot$ (*dashed* and *dotted curves*) and $a = 80\,R_\odot$ (*solid* and *dot-dashed curves*). These are compared with locations of RS CVn binaries (*circles* are data from Fekel et al. 2002; Morel et al. 2004; Fekel & Henry 2005). *Solid and dashed curves* start with a subgiant model having $R = 3\,R_\odot$ and $\Omega = 0$, while *dot-dashed and dotted curves* initially (at $R = 3\,R_\odot$) have $\Omega_{-5} = 2.5$, which extrapolates to $v_{\rm rot} \approx 100$ km s^{-1} back on the ZAMS. The evolution of $v_{\rm rot} = R\,\Omega$ and a due to the tidal interaction is followed by solving equations $(7\!-\!8)$ as described in text.
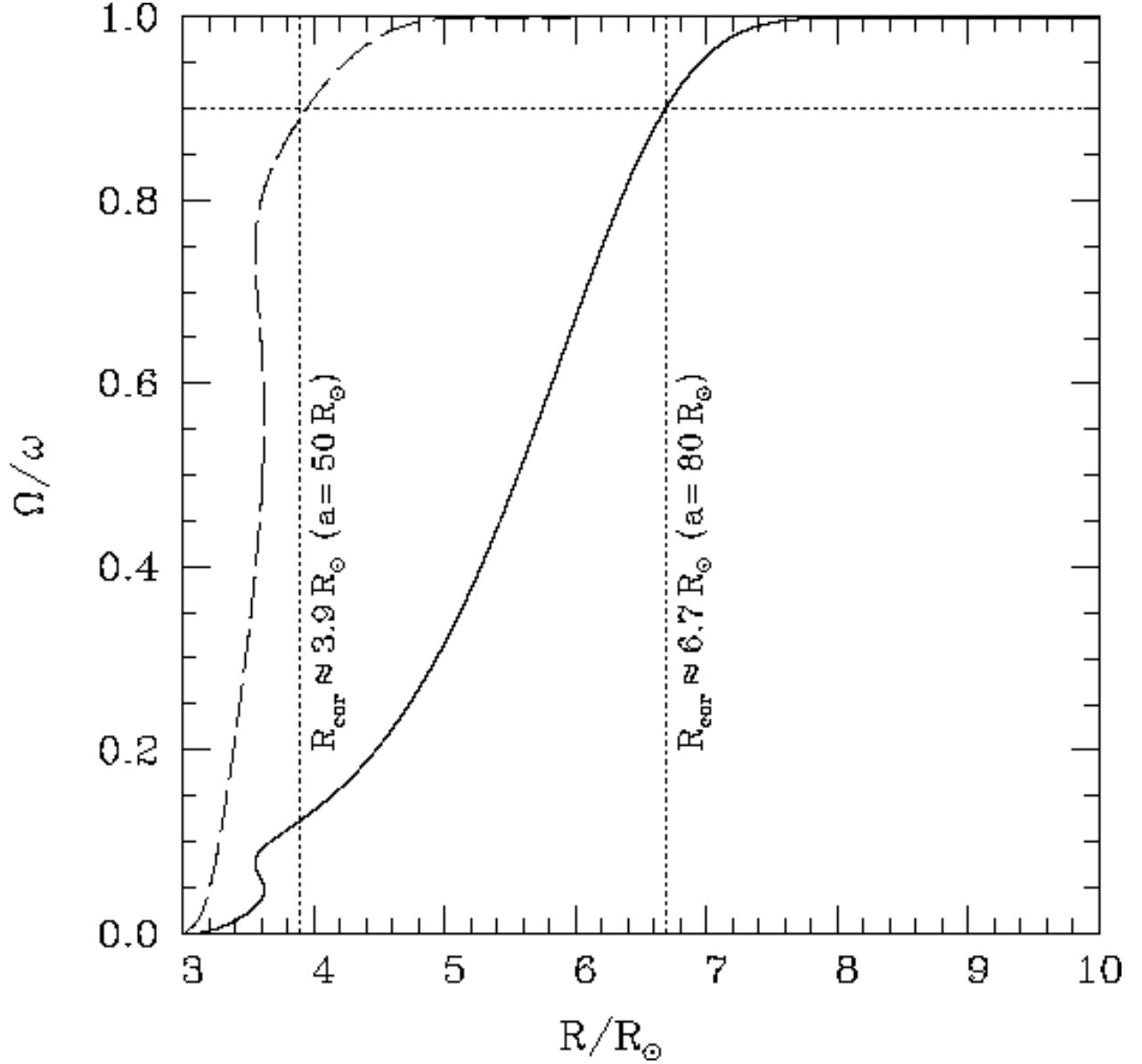
Fig. 13.— Tidal evolution of the ratio of the spin and orbital angular velocities for a solar-metallicity $1.7\,M_\odot$ primary star in a binary system with the same $q = 0.5$ but different semi-major axes: $a = 50\,R_\odot$ (*dashed curve*) and $a = 80\,R_\odot$ (*solid curve*). We define the corotation radius $R_{\rm cor}$ as the radius at which $\Omega/\omega = 0.9$. During the subsequent evolution of the primary star it is assumed that the part of its convective envelope above $R_{\rm cor}$ rotates as a solid body with $\Omega = \omega$, while the part at $R_{\rm BCE} \leq r \leq R_{\rm cor}$ still rotates differentially.
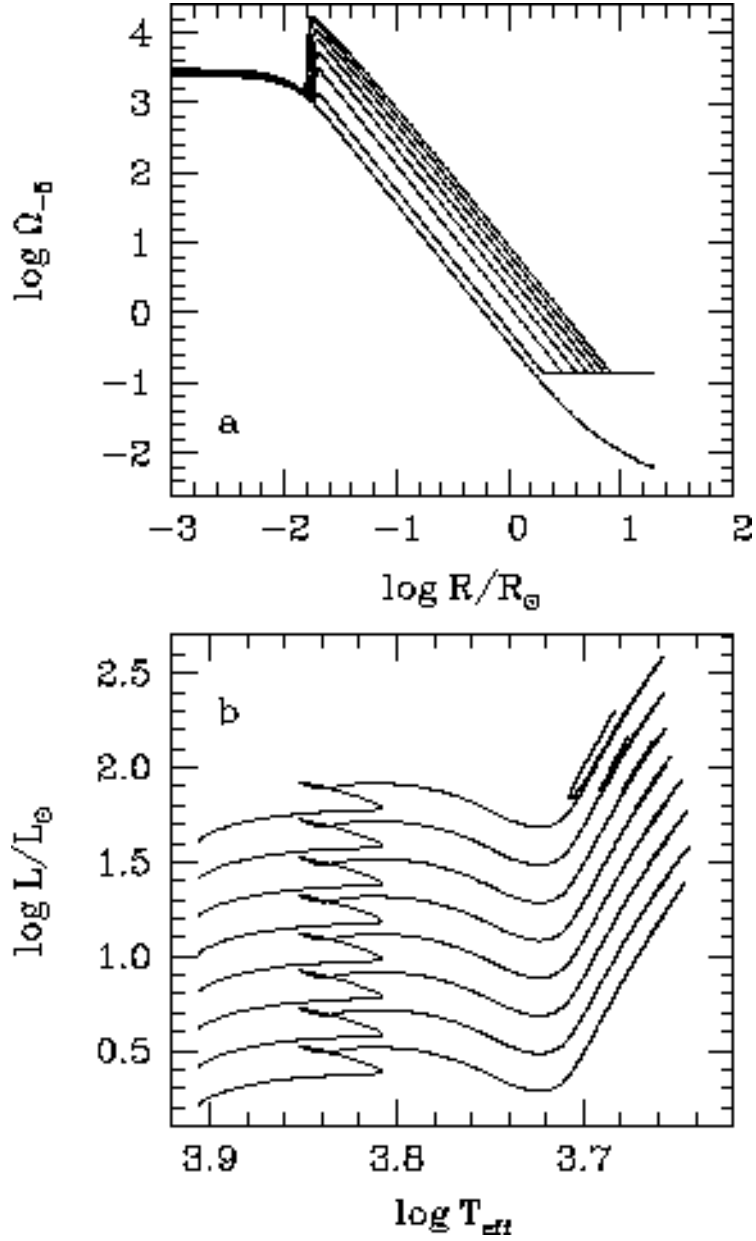
Fig. 14.— The single and binary evolutionary models of a solar-metallicity $1.7\,M_\odot$ star with the corotation radii $R_{\rm cor}/R_\odot = 2$, 3, 4, 5, 6, 7, and 8 (from bottom to top). The increase of $R_{\rm cor}$ causes the radiative zone to spin up (panel a), which makes effects of rotation on the model's internal structure to be more pronounced, resulting in a noticeable extension of the bump luminosity zigzag (panel b; in order not to overlap each other, the tracks are shifted along the ordinate).
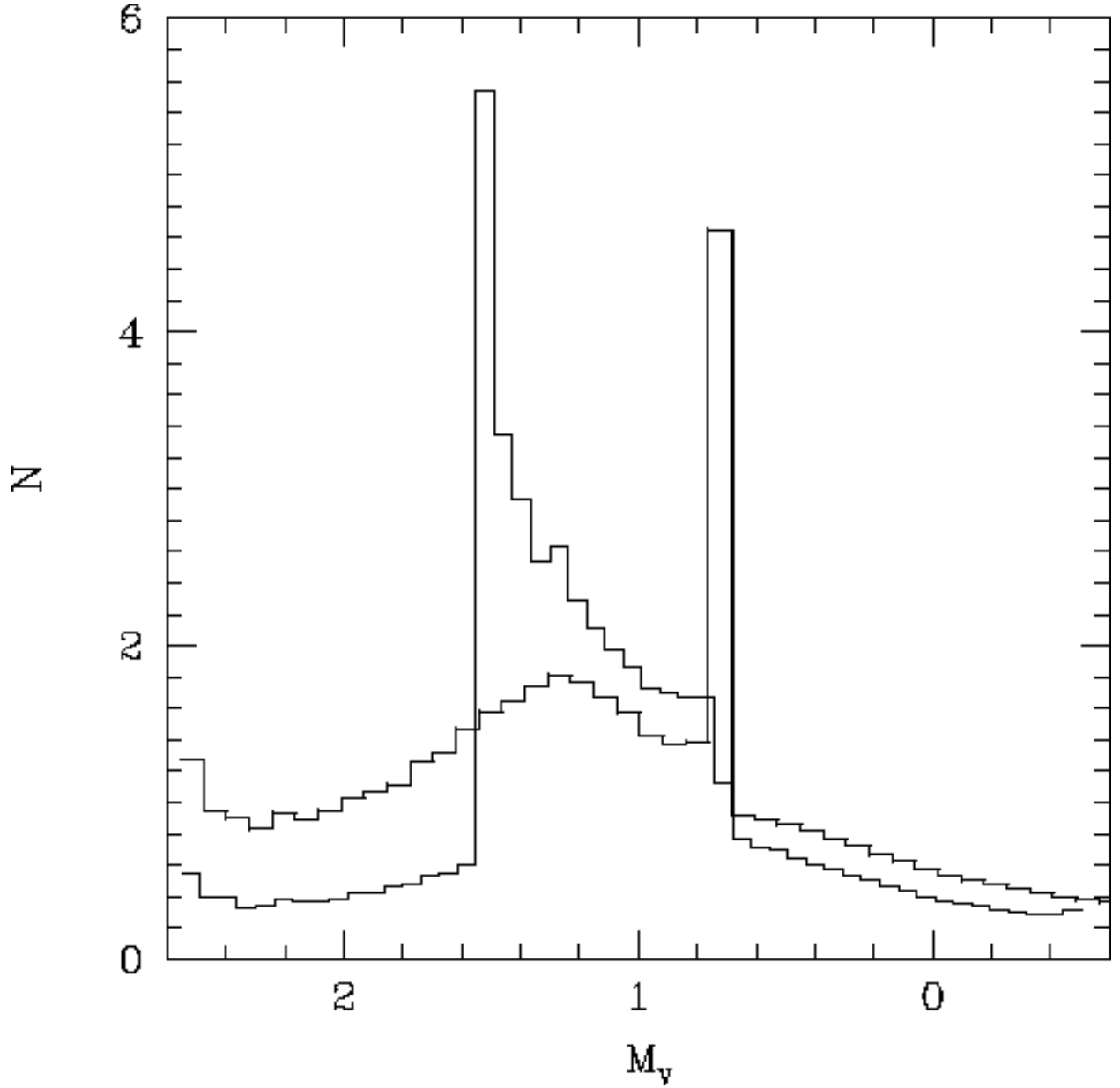
Fig. 15.— Differential luminosity functions constructed using the evolutionary track of the single solar-metallicity $1.7\,M_\odot$ star (*thick curve*) and the track of the same star placed into the binary system with $q = 0.5$ and $a = 80\,R_\odot$ (*thin curve*). The time spent by the single star between $M_V = 2$ and $M_V = 0$ is 109 million years, while for the binary star it takes 146 million years to make an extended zigzag on the CMD when M_V increases from 0.71 to 1.52 and then decreases back to 0.71. For the binary star, the bump luminosity is shifted towards the lower RGB by $\Delta M_V \approx 0.8$.
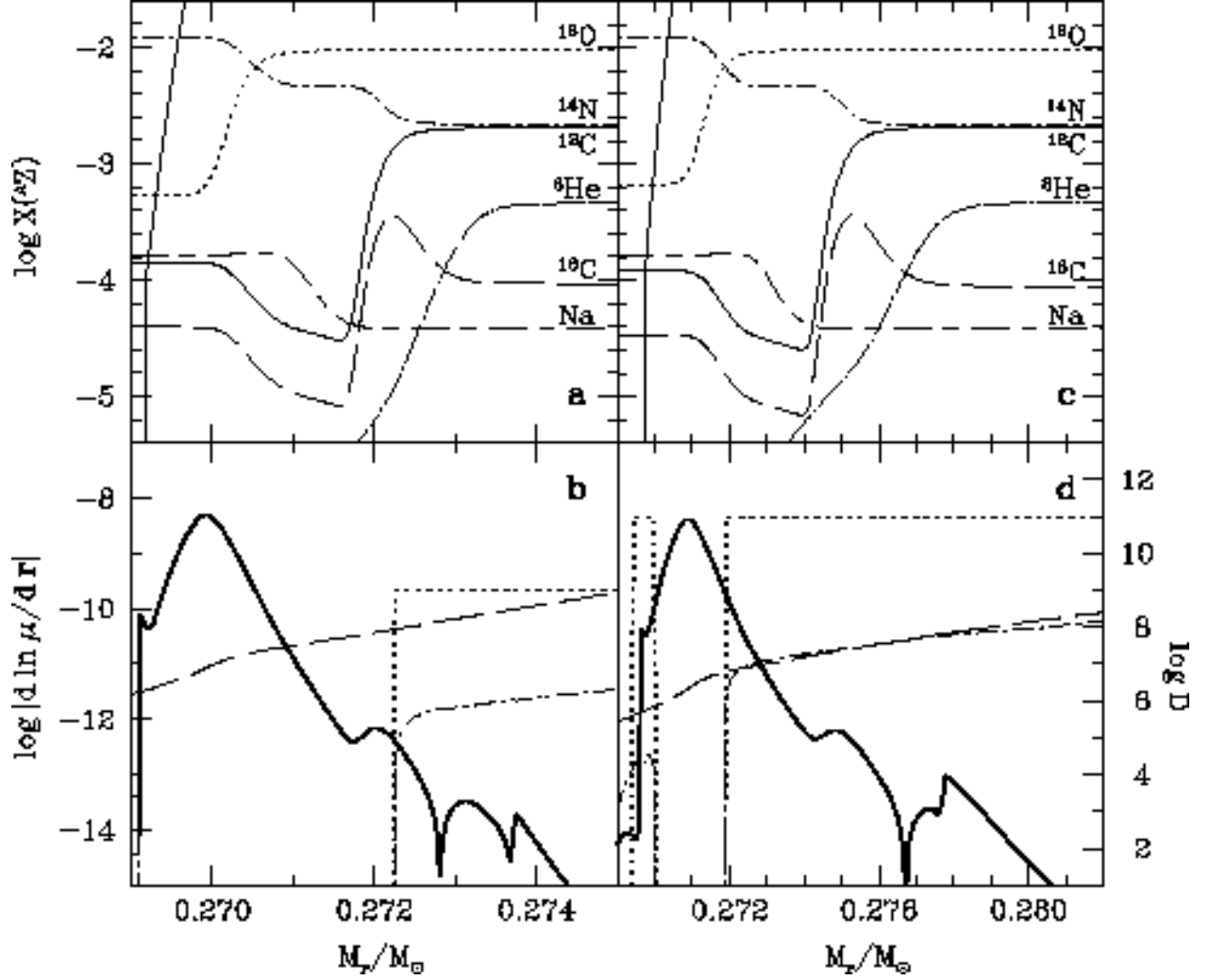
Fig. 16.— Profiles of some element abundances (panels a, c) and diffusivities (panels b, d) in the single solar-metallicity $1.7\,M_\odot$ model star (panels a, b) and in the same model placed into the binary system with $q = 0.5$ and $a = 80\,R_\odot$ (panels c, d). Both models are beyond the bump luminosity. In panels b and d, *dot-dashed curves* show the turbulent diffusion coefficient (1) for $f_v = 1$, *dashed curves* — thermal diffusivity, *solid curves* — μ-gradients, and *dotted curves* — constant diffusion coefficients for canonical ($D_{\mathrm{mix}} = 10^9$ cm^2 s^{-1}, panel b) and enhanced extra mixing ($D_{\mathrm{mix}} = 10^{11}$ cm^2 s^{-1}, panel d). The mixing depth is always constrained by equation (4).
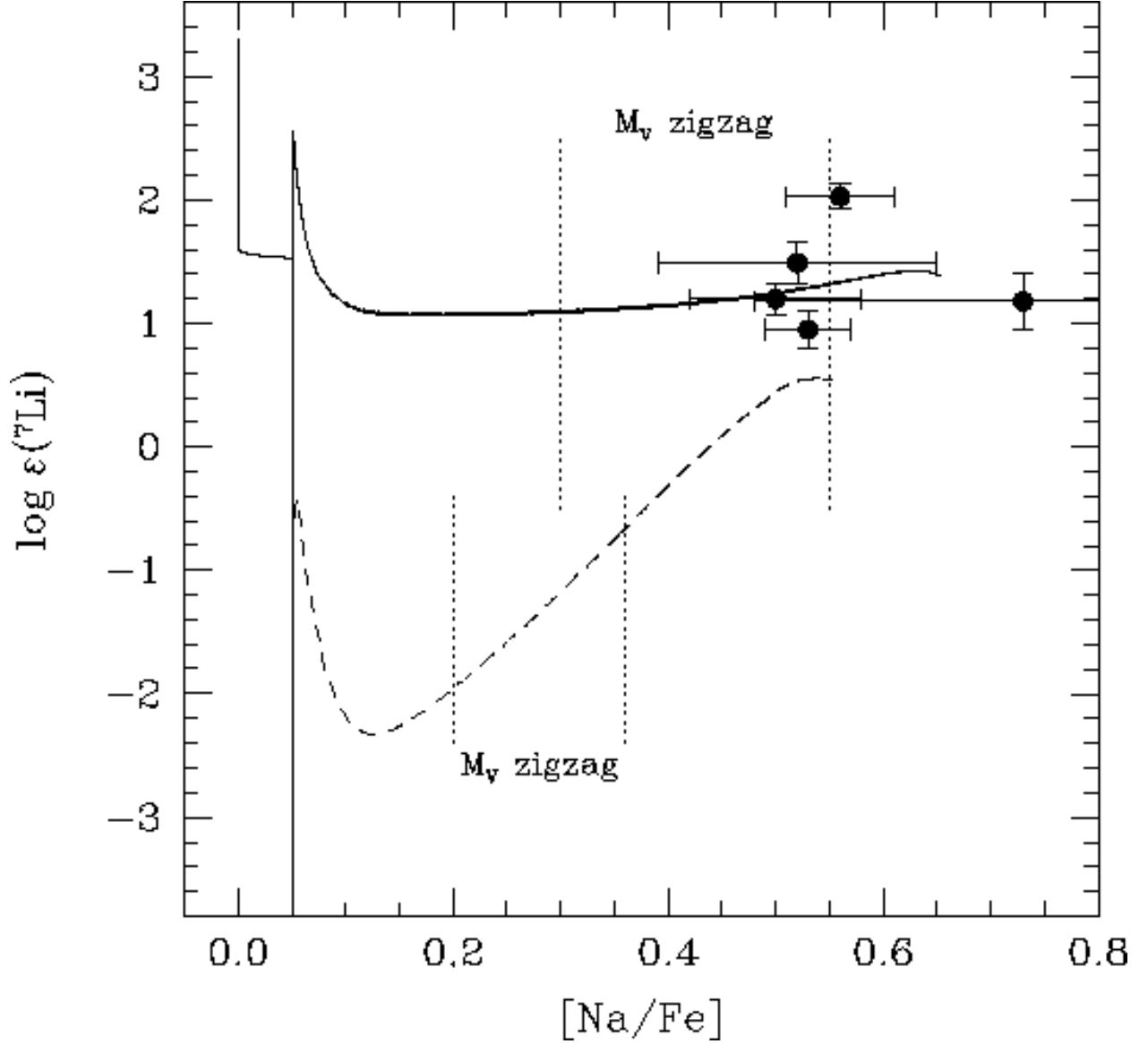
Fig. 17.— Peculiar combinations of the Li and Na abundances in RS CVn binaries (*circles*), as reported by Morel et al. (2004), and their theoretical reproduction with our model of enhanced extra mixing in the solar-metallicity $1.7\,M_\odot$ binary red giant. *Dashed curve* is obtained using the diffusion coefficient (1) with $f_\mathrm{v} = 20$, *solid curve* — for the constant coefficient $D_\mathrm{mix} = 10^{11}$ cm^2 s^{-1} with the mixing depth from equation (4). *Dotted line segments* delimit regions of the bump luminosity zigzag extended by fast rotation.
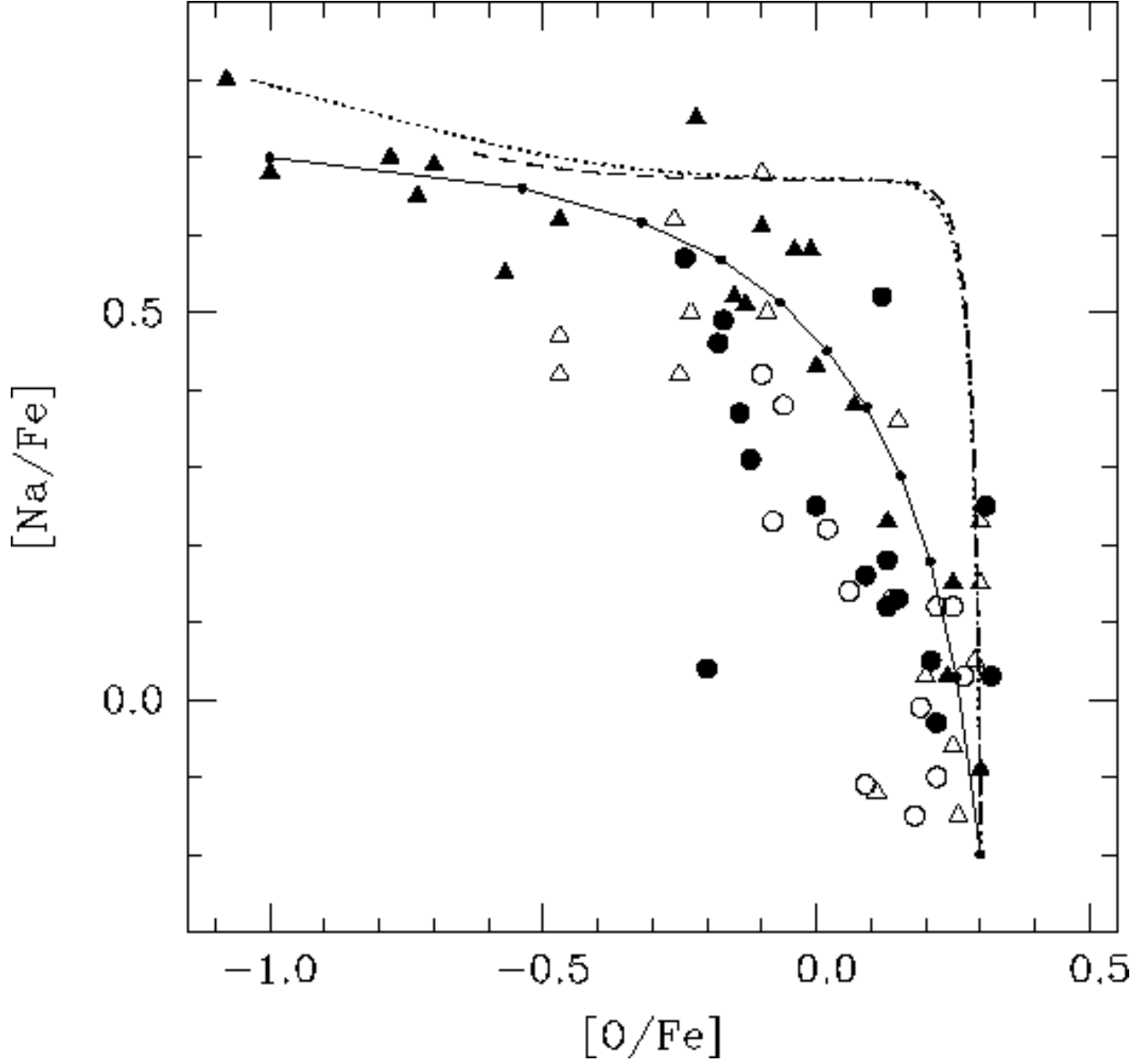
Fig. 18.— The O–Na anticorrelation in red giants in the globular clusters M3 (*circles*) and M13 (*triangles*) from a recent update by Sneden et al. (2004). *Filled symbols* — stars with lower surface gravities (higher luminosities). *Solid curve* shows a simple mixture of a $(1-x)$-fraction of material with the abundances $[O/Fe]_{init} = 0.3$, $[Na/Fe]_{init} = -0.2$ and a x-fraction of material with $[O/Fe]_{acc} = -1.0$, $[Na/Fe]_{acc} = 0.7$ (*thick dots* on the curve mark values of x from 0 to 1 with the increment 0.1). *Dashed curve* is obtained with our model of tidally enforced enhanced extra mixing in a red giant with $M = 1.0\,M_\odot$, $Y = 0.24$, $Z = 0.0005$ and $f_\varepsilon = 0.0003$ in a binary system with $q = 0.3$ and $a = 50\,R_\odot$. It is computed using the diffusion coefficient (1) with $f_v = 20$. *Dotted curve* presents a test case in which Ω in the radiative zone has been increased by the factor of 25 as compared to the single star case.
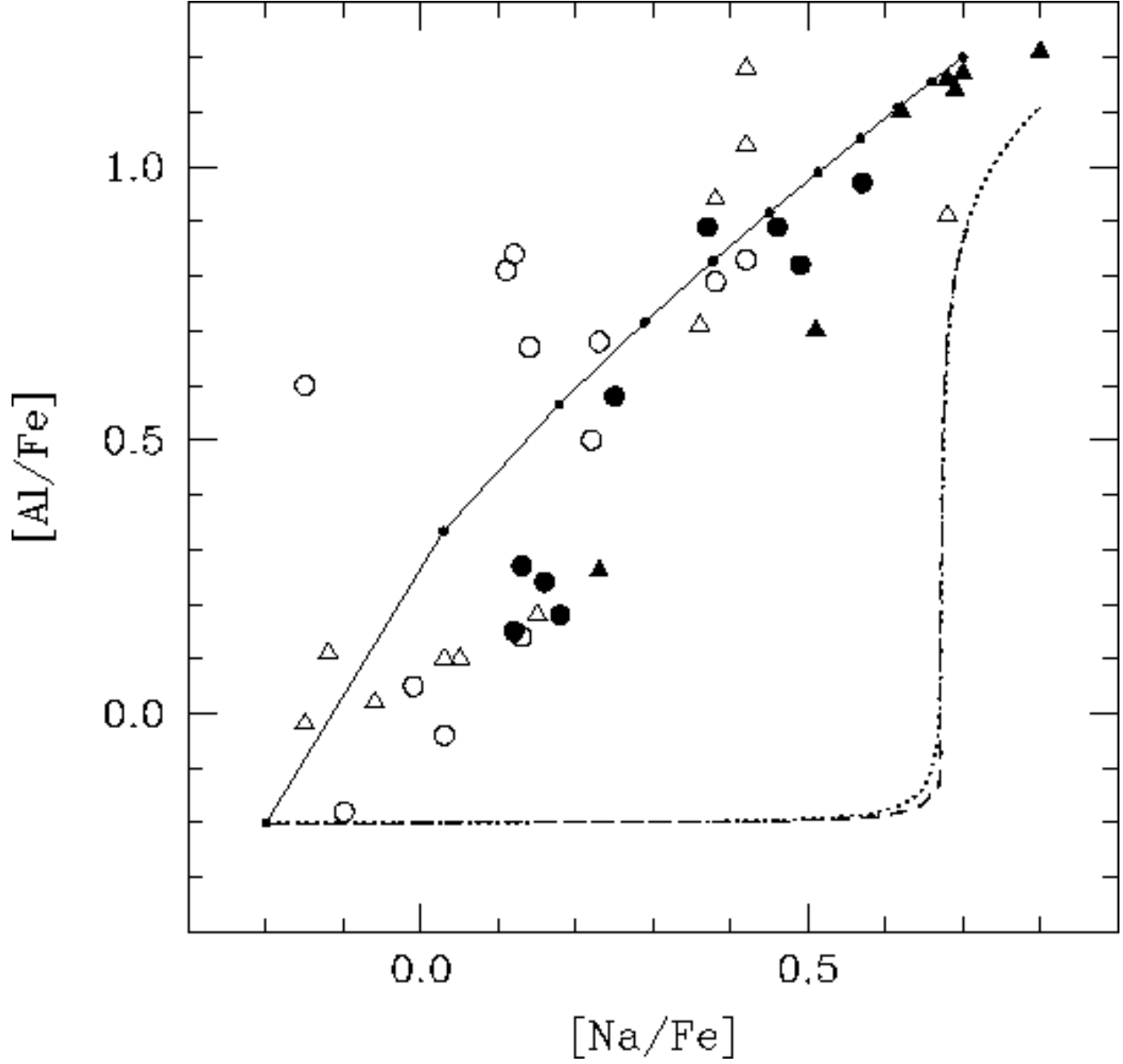
Fig. 19.— The same as in Fig. 18 but for the Na–Al correlation. For Al, the initial and most extreme abundances are $[\text{Al/Fe}]_{\text{init}} = -0.2$, $[\text{Al/Fe}]_{\text{acc}} = 1.2$. Following Denissenkov & Tout (2000), we have additionally assumed that $[^{25}\text{Mg/Fe}]_{\text{init}} = 1.2$ and the rate of reaction $^{26}\text{Al}^{\text{g}}(\text{p},\gamma)^{27}\text{Si}$ is a factor of 10^3 as fast as its rate from Angulo et al. (1999).